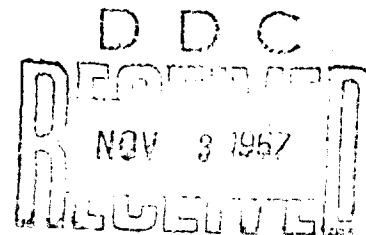AD660531

Experimental Evaluation of Flush Electrostatic Probes for Reentry Measurements

---

JULY 1967

Prepared by W. P. THOMPSON
Aerodynamics and Propulsion Research Laboratory
Laboratory Operations
AEROSPACE CORPORATION

D D C

NOV 3 1967

EXPERIMENTAL EVALUATION OF FLUSH ELECTROSTATIC
PROBES FOR REENTRY MEASUREMENTS

Prepared by

W. P. Thompson
Aerodynamics and Propulsion Research Laboratory

Laboratory Operations
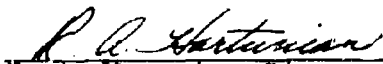AEROSPACE CORPORATION

July 1967

FOREWORD

This report is published by the Aerospace Corporation, El Segundo, California, under Air Force Contract No. F04695-67-C-0158.

This report, which documents research carried out from July 1966 through March 1967, was submitted on 29 August to Captain John T. Allton, SMTRE, for review and approval.

The author is indebted to P. M. Chung and K. E. Starner for many helpful discussions, and to K. E. Starner and D. J. Spencer for their development of the arc-channel facility. C. Gaulin and R. Rossi of the Materials Sciences Laboratory provided samples of CP and BeO for testing. The able assistance of C. E. Gardner, H. Bixler, and T. Felker in the performance of the experiments is appreciated.

Approved

R. A. Hartunian
R. A. Hartunian, Director
Aerodynamics and Propulsion
    Research Laboratory

Publication of this report does not constitute Air Force approval of the report's findings or conclusions. It is published only for the exchange and stimulation of ideas.

John T. Allton
John T. Allton
Captain, United States Air Force
Chief, Applied Mechanics Branch

-ii-

ABSTRACT

The current collection characteristics of flush-mounted electrostatic probes were determined in a simulated reentry boundary layer flow. The thermochemistry and fluid dynamic profiles on sharp cones at 180 to 100 kft altitude are simulated by a subsonic flow of arc-heated air in a $1/2 \times 2$ in. cooled channel. The experimentally determined probe currents are correlated with the known channel electron densities using two theoretical models developed by Chung and Bredfeldt et al. It is found that for electron densities of order $10^{10} - 10^{13}$ Chung's theory correlates the data well. High temperature materials were tested, and stainless steel electrodes in pyrolytic boron nitride insulators are recommended for operation up to surface temperatures of $1400°K$. Comparison of the two theoretical models in predicting flight performance shows them in excellent agreement for sodium-contaminated ablating cones below 175 kft. For the low electron densities on sharp cones in clean air, neither theory is valid above 115 kft altitude. Detailed graphs and tables of flight environment, materials properties, and probe electrical characteristics are presented.

CONTENTS

TABLES

FIGURES

NOMENCLATURE

a   radius of disc probe element

A   area of probe; thermionic emission constant, $60 \text{ amp/cm}^2 \,^\circ\text{K}$
(Fig. 25)

$\hat{A}$ Chung's parameter for sheath/B. L. thickness, Eq. (6)

c   distance between centers of probe elements

Cp   specific heat

d_s sheath thickness, Eq. 5

D   diffusion coefficient

e   electronic charge, 1.6×10^{-19} coulomb

E   electric field strength, volt/cm

h   altitude; specific enthalpy

I   electric current collected by probe

J   current density I/A, amperes/cm^2

k   Boltzmann constant, 1.38×10^{-16} erg/$^\circ$K

K   thermal conductivity; mobility

l Chapman-Rubesin parameter $(\rho_w \mu_w / \rho_o \mu_o)^{0.2}$

L   length of probe parallel to flow; mean free path

m   particle mass

$\dot{m}$ mass flow rate

n   particle number density

p   pressure

Pr   Prandtl number $\mu / \rho K$

$\dot{q}$ heat flux

Q   collision cross section

R   resistance, ohms

Sc   Schmidt number, $\mu/\rho D$

T   temperature (°K or °C as noted)

t   thickness of insulator

U   Reentry velocity

u   flow velocity

V   bias voltage

v   mean thermal speed, Eq. (4)

W   width of probe element transverse to flow

x   distance from nose of vehicle

y   distance normal to wall

Δ Chung's B. L. thickness, Eq. 7

δ geometric B. L. thickness, $u/u_\infty = 0.99$

ϵ_o permittivity of free space, 8.85×10^{12} farad/m

η similarity parameter, Eq. (8)

λ free space wavelength of microwave beam

Λ Debye length, Eq. (6)

μ viscosity

ν collision frequency

ρ mass density; electric resistivity

σ electric conductivity

ϕ thermionic work function, electron volts (note K/e = 11,600°K)

Subscripts

b	bias (voltage)
e	electron
g	neutral gas
i	ion
m	momentum transfer
o	evaluated at B. L. temperature peak (or at electron peak, assumed equivalent)
s	evaluated at sheath edge
sat	saturated
th	thermal
w	evaluated at wall
δ	evaluated at B. L. edge
∞	free stream
conv	convected contribution to current
tot coll	assuming all ions removed from B. L.
tot	total current collected, drift + convection

1. INTRODUCTION

The flush-mounted electrostatic probe is of great interest for the measurement of boundary layer electron density on reentry vehicles (Refs. 1 and 2). It causes no flowfield disturbance, has high sensitivity and wide dynamic range, and is mechanically and electrically simple. The theory of current collection by surface electrodes through boundary layers is not well understood, however, and it is the purpose of this work to compare probe performance in a simulated reentry boundary layer flow with two existing theoretical models. In addition, the close simulation of boundary layer profiles and surface temperature achieved in the arc-fed channel flow facility employed provides a realistic preflight evaluation of probe geometry, materials, and electrical characteristics.
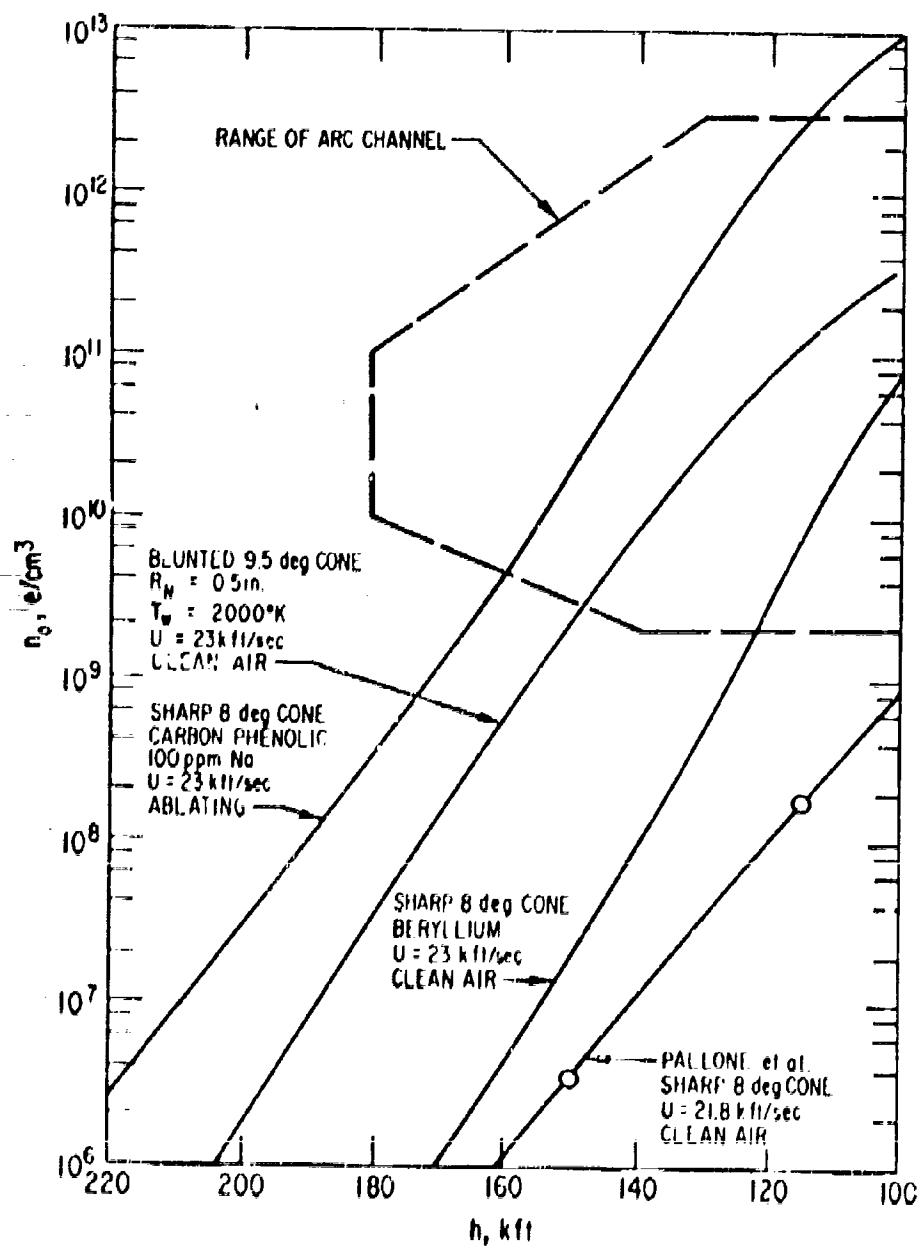
Figure 1. Peak Electron Density in the Boundary Layer of Reentering Cones

II. REENTRY ENVIRONMENT

The reentry environment experienced at the surface of typical conical bodies is shown in Figures 1-3. The boundary layer peak electron density, surface temperature, and heat transfer rate are indicated as functions of altitude.[1] Boundary layer profiles of temperature, density, and electron concentration at two altitudes (Ref. 3) are shown in Figures 4 and 5. In subsequent analysis, it will be assumed that at altitudes above nominal transition (100 kft), the profiles in contaminated air are similar to the clean air curves, differing only in the magnitude of electron concentration. Although the conditions of flight for Figures 1, 4, and 5 are not identical, the boundary layer profiles are fairly insensitive to small velocity differences. Thus we require the electrostatic probe to measure electron densities from 10^6 to 10^{13} and to withstand surface temperatures up to 2000°K.

In order to establish the feasibility of the flush probe, we have performed a laboratory calibration designed to simulate the essential features of the reentry environment. We shall discuss the flow facility, its simulation and diagnosis; flush probe geometry, circuitry, and high temperature materials; theories of probe operation; experimental results; and finally, prediction of flight performance and recommendations for further development.

---

[1]R. B. Selberg, Aerospace Corp., San Bernardino, Calif., private communication.
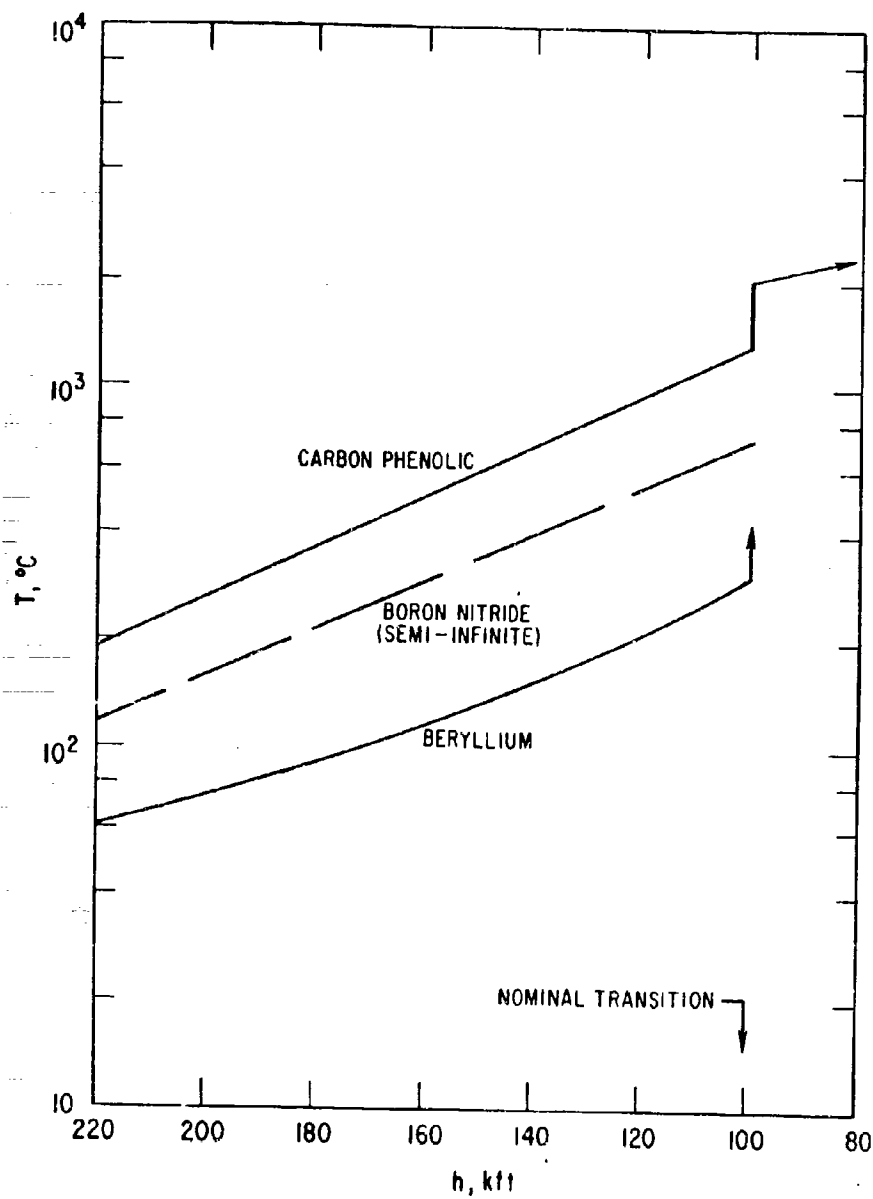
Figure 2. Surface Temperature of Reentering Cones
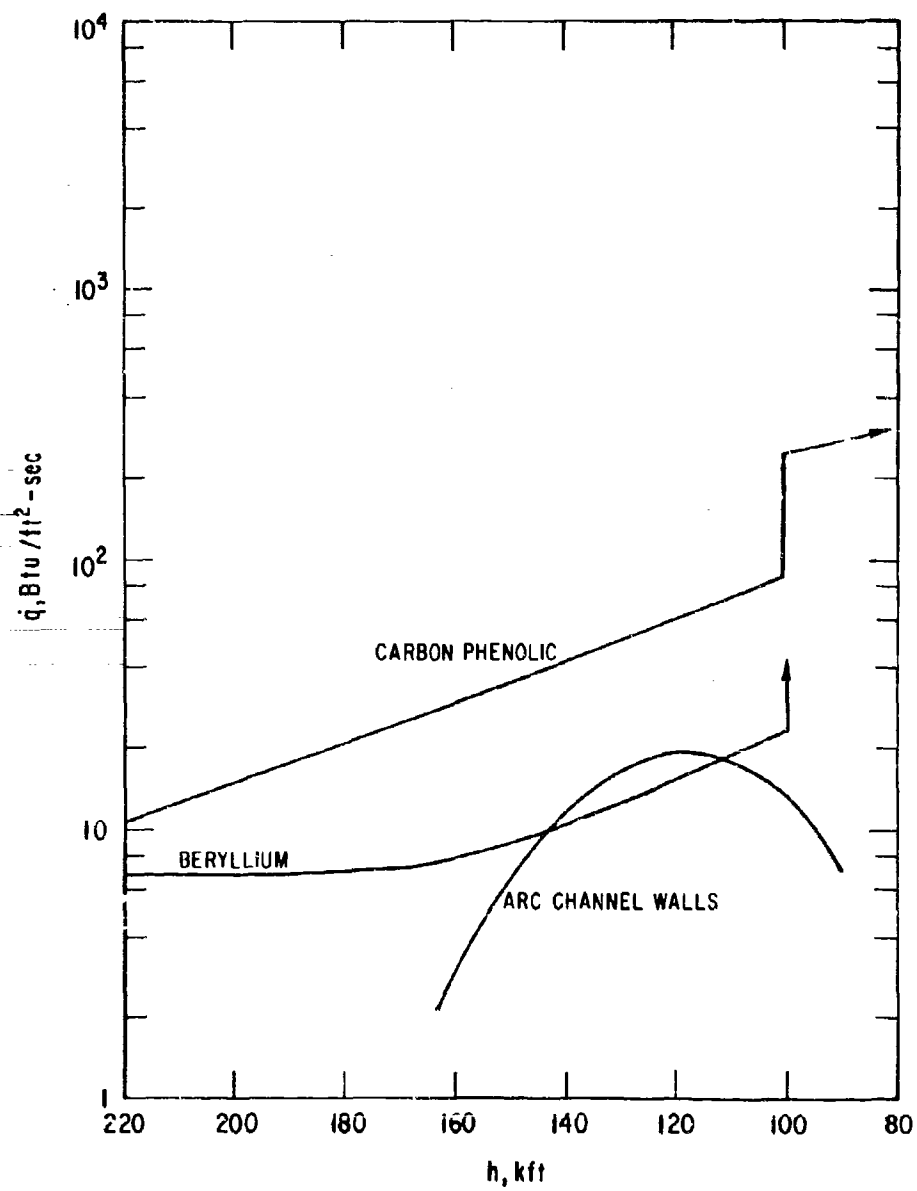
Figure 3. Heat Flux to Surface of Reentering Cones
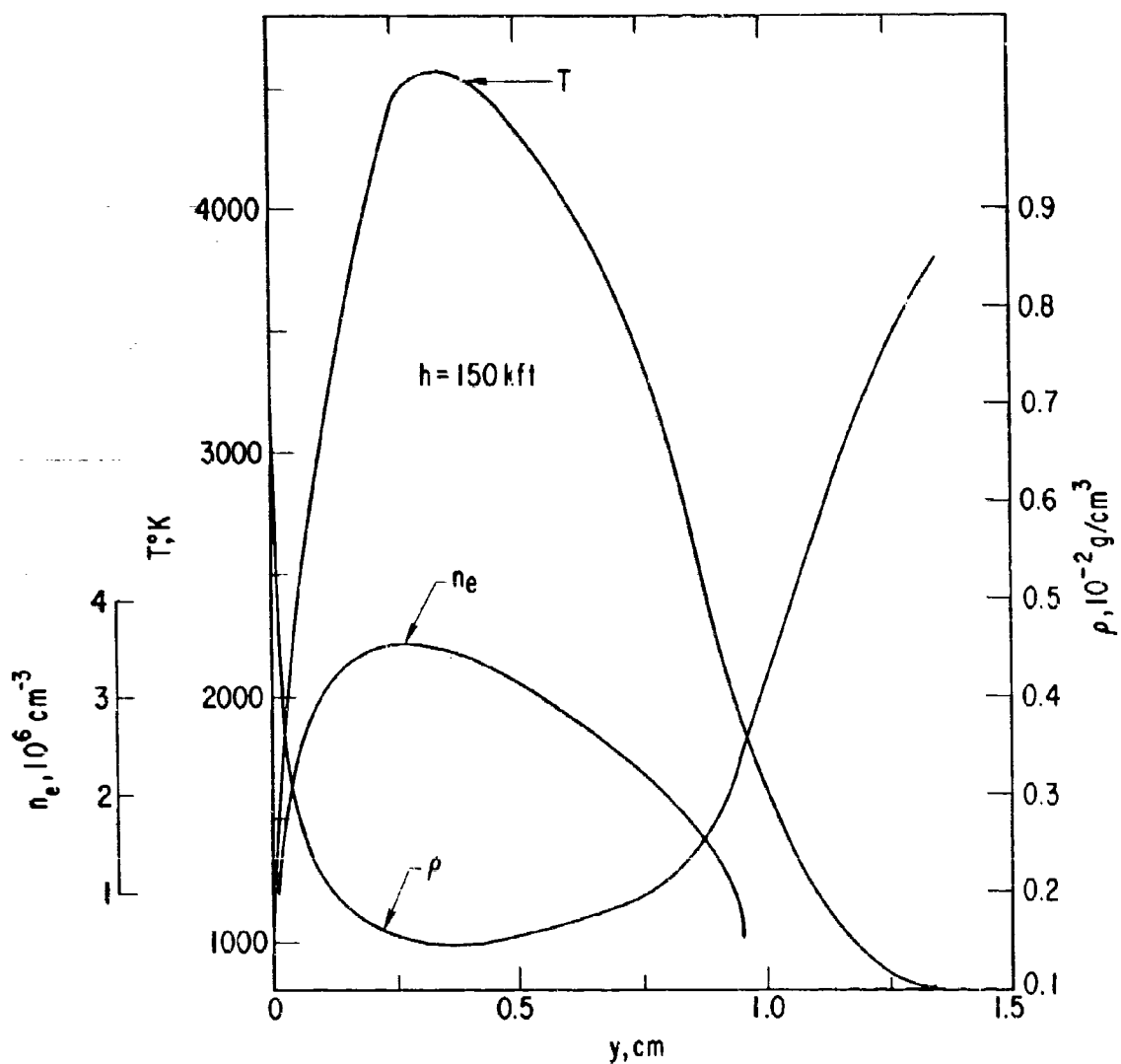
Figure 4.   Boundary Layer Profiles on 8-deg Cone at 150 kft
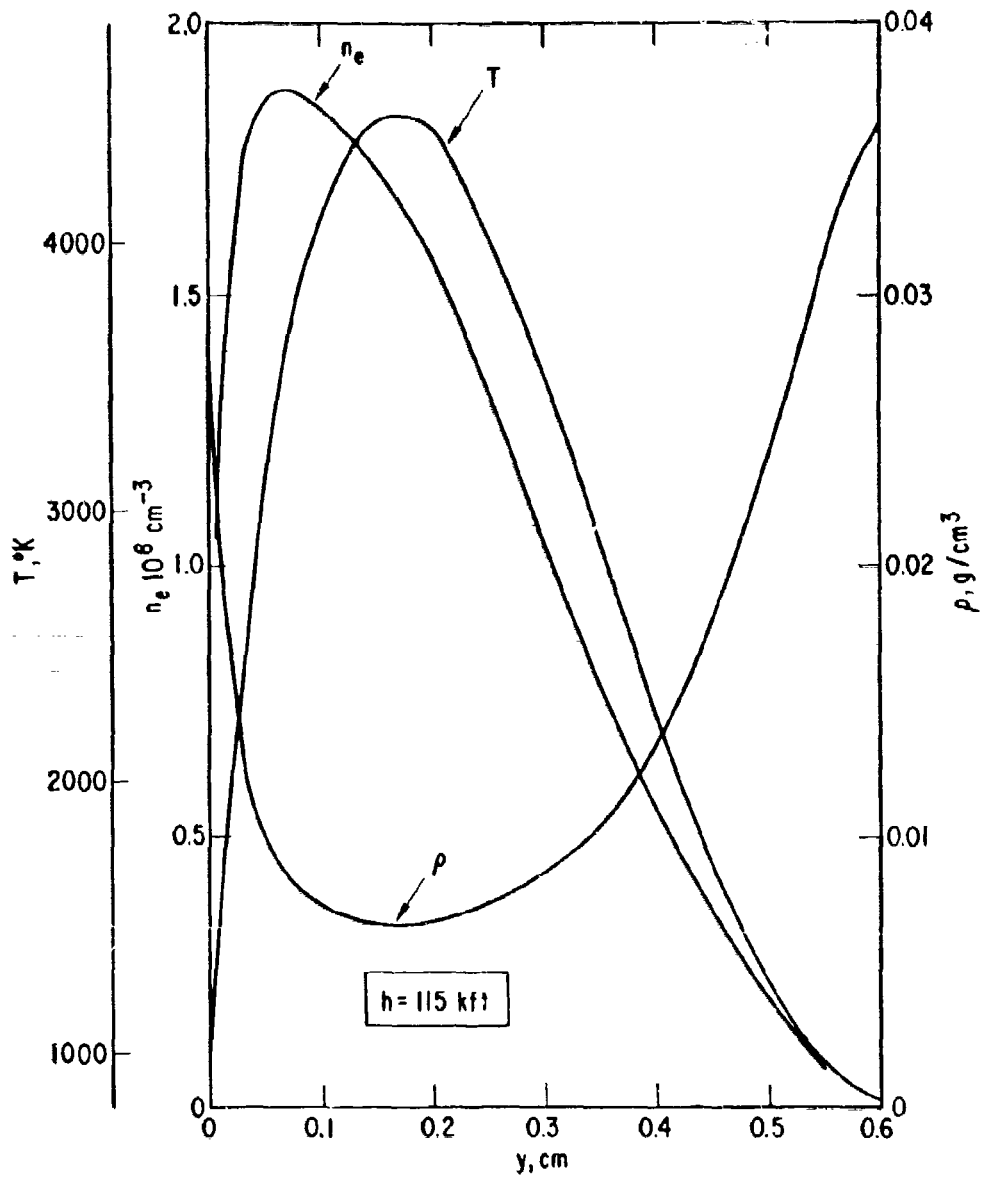
Figure 5. Boundary Layer Profiles on 8-deg Cone at 115 kft

Figure 6. Arc-channel and Instrumentation Schematic

III. ARC-CHANNEL FLOW FACILITY

We wish to simulate the boundary layer thickness, temperature, density and electron concentration profiles, and chemical composition. The facility developed (Ref. 4) is shown in Figures 6 and 7. A fully developed pipe flow is established between cold walls in a rectangular channel, fed by a subsonic 200 kw arc-jet flow. Nitrogen fed through the swirling arc is mixed with cold oxygen tangentially injected in the plenum chamber. The mixing has been checked by time-averaged mass spectrometer sampling downstream of the plenum. Our nominal plenum condition is 40 torr at 6000°K. From the plenum exit nozzle, a constant area transition to the $1/2 \times 2$ in. rectangular channel is made. Traverses of total pressure and ion current to a stagnation Langmuir probe (Ref. 5) were made in the 2-in. direction with a water-cooled probe. Three-point profiles were obtained in the 1/2-in. direction with uncooled pressure and Langmuir probe rakes rapidly injected and removed from the flow after initial stabilization by means of a sliding channel section. Average enthalpy at the test section (nominally 3000 Btu/lb) was obtained from heat balance on the individual channel sections and at the exit. Using the known mass flow, static pressure, average enthalpy, and total pressure profile, we use the Crocco integral technique to iterate upon assumed velocity and static temperature profiles until a consistent set is obtained. Profiles of u, ρ, T, and n_e at a typical test point are shown in Figure 8. A range of static pressure from 15 to 150 torr, peak n_e from 10^{10} to 10^{12} cm^{-3}, and centerline gas temperature from 3500 to 5500°K can be obtained. The thickness of 1/2 in. was chosen to simulate the boundary layer at about 150 kft. The density, temperature, and velocity profiles in flight are, of course, not symmetric, but the important interaction is that between the wall-mounted electrostatic probe (Ref. 2) and the profile out to peak n_e; the remainder of the profile need not be simulated in detail. The arc-channel flow thus simulates quite accurately the thermochemical properties, thickness, and profiles of the reentry boundary layer. The velocity is not
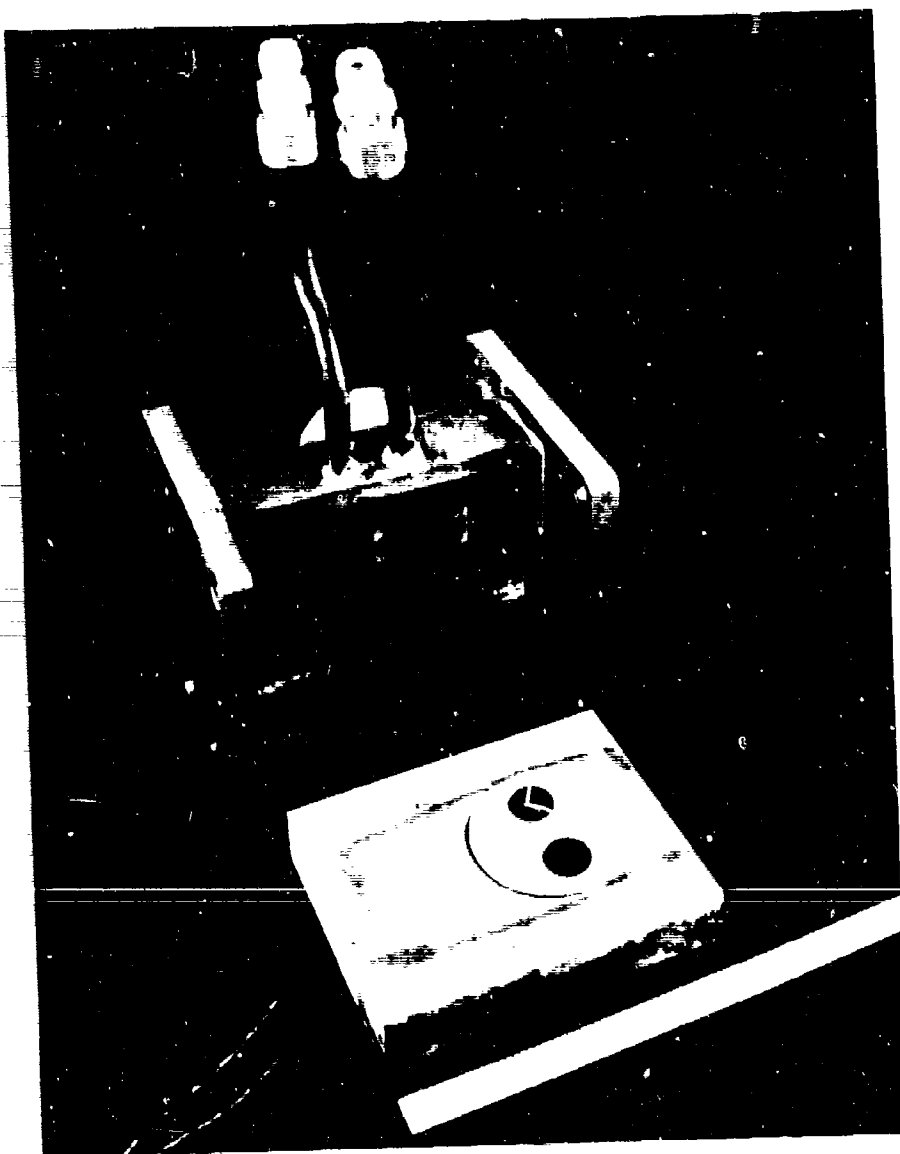
Figure 7.   Arc-channel Test Section, Showing "Plug" and
Wall-mounted "Disc" Probes and X-band
Microwave Window
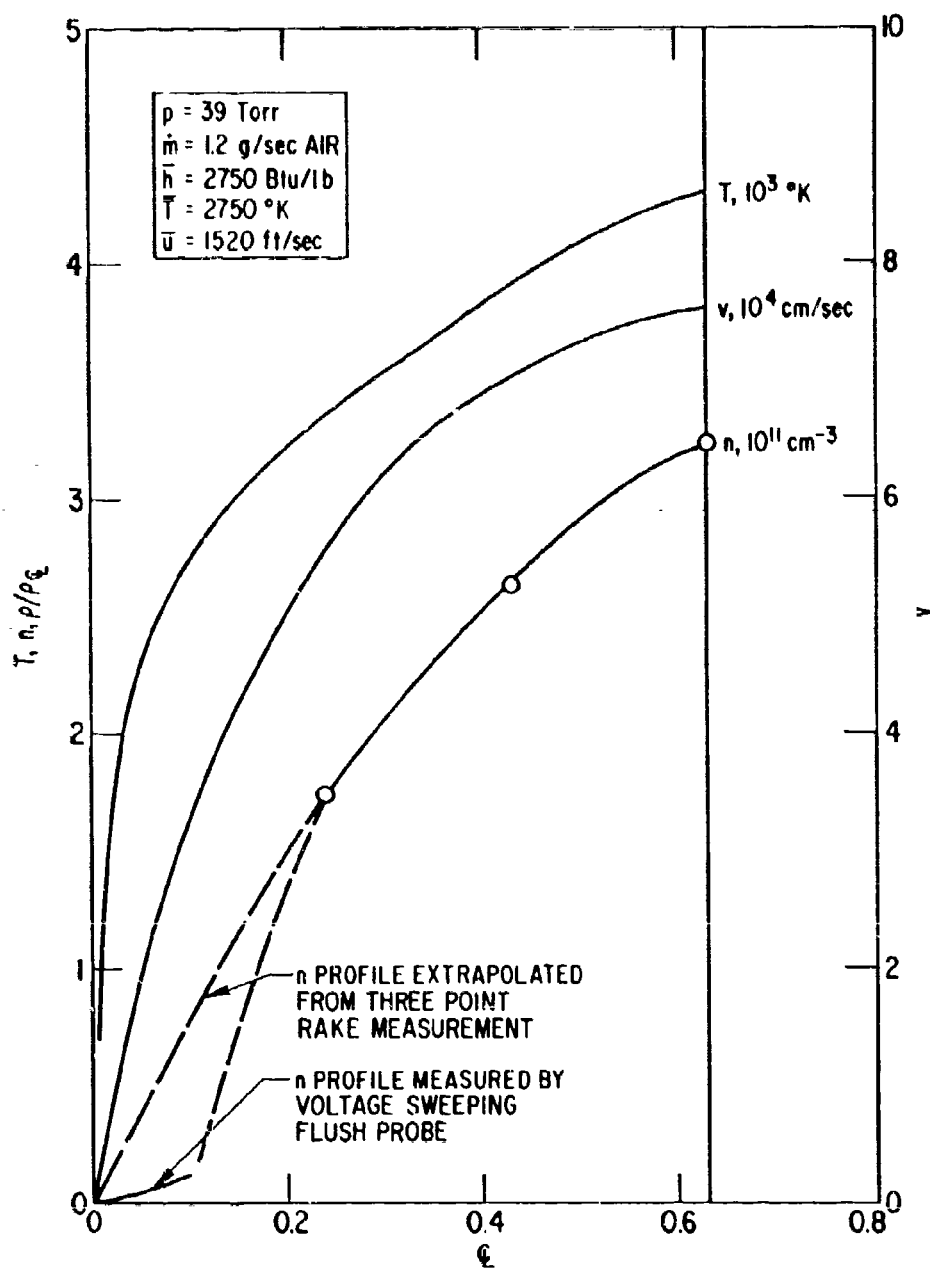
Figure 8.   Arc-channel Profiles in 1/2-in. Dimension at
Nominal Test Point

simulated, since it is of the order of 1500 fps in the channel (Mach number ≤ 0.3 based on mean velocity and mean temperature). However, it will subsequently be shown that over a significant range of probe operation, the boundary layer velocity profile does not affect the probe operation so long as n_e and ρ profiles are correct.

Electron density was measured on the channel centerline with the stagnation Langmuir probe (Refs. 5 and 6), and an integrated value was obtained by x-band microwave interferometry (Ref. 7). Numerical calculations of phase shift, transmission, and reflection coefficients[2] for several assumed profiles were compared with measured values to establish average electron number density in the channel. Within the errors of measurement (± 30 percent), no difference in the inferred centerline n_o among assumed flat, triangular, or parabolic n_e profiles could be detected. The microwave and Langmuir probe results were in good agreement, and microwave was used routinely. It was assumed for data reduction that the peak electron density was twice the average (integrated) value determined from the microwave, as is borne out by the measured Langmuir probe 3-point profiles. It should be noted that the microwave propagation geometry is not plane wave as assumed in the numerical calculations. However, for thin slabs ($\delta < \lambda$), experiments performed by the author have shown no systematic differences between the results obtained with the slot aperture shown in Figure 7 and those found with large-aperture horns through quartz channel walls, for which the plane wave assumption is fairly good. Also, calibration on slugs of known dielectric constant inserted in the channel gave results within 20 percent of the known values. All windows and dielectric channel walls in the path of the microwave beam are chosen to be halfwave plates and are hence practically invisible to the wave.

_____

[2] A numerical program has been developed by D. Kittel of the Aerospace Corp. Computation and Data Processing Center.

The flow is presumed to be in chemical equilibrium. No theoretical solution presently exists for reacting compressible laminar pipe flow with large heat transfer and diffusion; such a solution is required for exact analysis. Consideration of the plenum conditions (Ref. 8) and calculation of recombination rates of O atoms and ionized species in the channel indicate that we should be at least near equilibrium. The flow is contaminated by copper and sodium, as confirmed by spectral study, and it may retain some nonequilibrium ionization level during its rapid cooling during passage down the channel. However, the measured electron density level is much lower at the channel center than local equilibrium calculations (Ref. 9), based on the T profile of Figure 8, would suggest. Since n_e must be decaying from the 6000°K plenum, we presume that electron chemistry is in equilibrium, strongly modified by diffusion to the walls. Hence the electron density levels are somewhat higher than nonequilibrium clean sharp cone calculations (Ref. 3) suggest, and are appropriate to those achieved in flight on blunted cones in clean air, or on contaminated ablating vehicles.

This arc-channel flow concept has been used by the author for a study of antenna breakdown during reentry (Ref. 10) and has been proposed for evaluation of microwave impedance probes (Ref. 11) and RF conductivity gauges (Ref. 12), and for thermal loading in antenna window materials studies. The heat flux measured at the test section of our arc-channel as a function of simulated density-altitude has been superimposed on Figure 2; higher q can be achieved at stations closer to the plenum. It was found that the inner surface of a 1/4-in. quartz wall could be brought to melting temperature (1200°K) after 100 sec of running. Thus, although the flight heat flux cannot be simulated well, realistic surface temperatures are attainable.
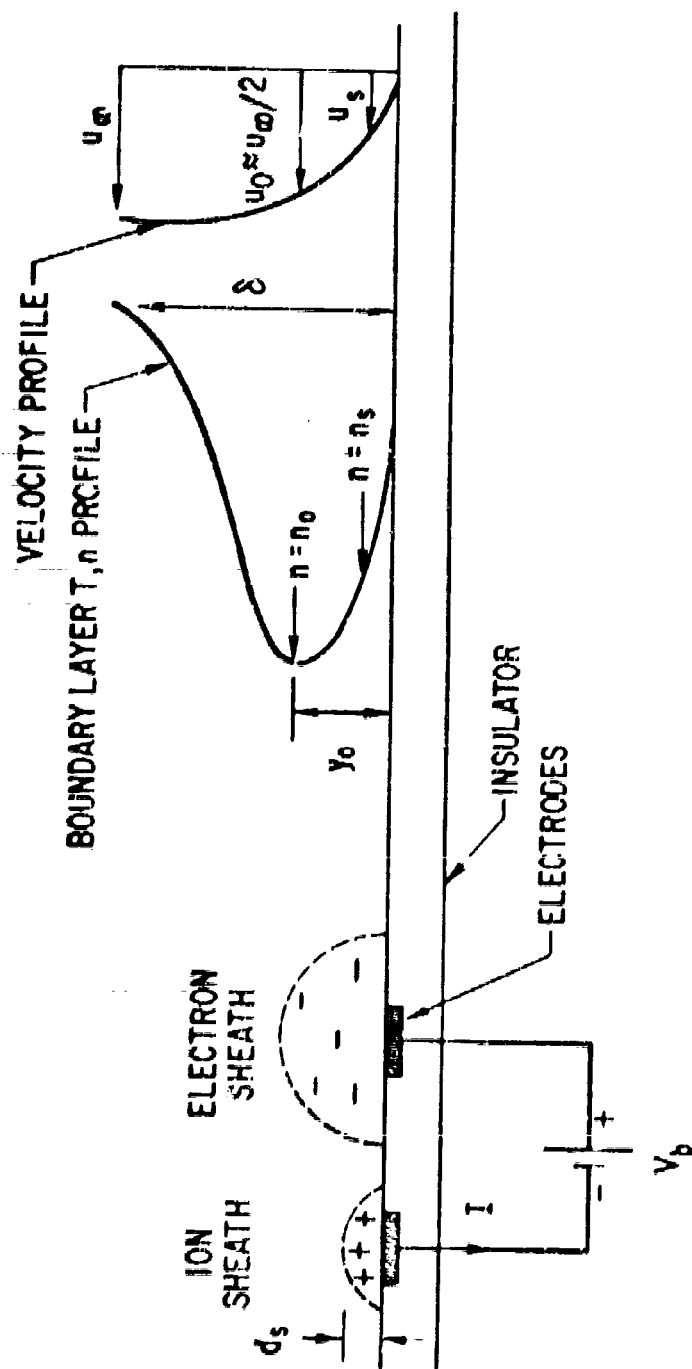
Figure 9. Schematic of Flush Electrostatic Probe in Boundary Layer, Showing Sheaths and Boundary Layer Profiles on Typical Hypersonic Cone

IV. PROBE CONSTRUCTION

The basic concepts of Langmuir probe operation have been covered in the literature (Refs. 13-15). The configuration as we wish to use it is shown in Figure 9. At high pressures ($d_s \gg L$) the space charge sheaths formed are mobility-limited (Ref. 17). The current collection through a collision-dominated sheath is not well understood, but the results of Ref. 1 seem to show that, at least approximately, the current at ion saturation is given by the classical value of random thermal drift at the sheath edge. Hence, although the concepts are not clearly defined, we shall discuss the flush probe as though it were of the classical Langmuir type.

Two plane metallic electrodes are set in a block of insulating material, which is then mounted flush with the wall of the arc-channel. In order for Chung's analysis (Ref. 2) to apply, the electrodes must be of dimensions δ and be separated by a distance δ or more from each other. We also wish to keep the electrode size large compared with a sheath thickness, so that any sheath area corrections will be small. We have employed the four geometries shown in Figures 7 and 10. The small plug probe (P) remains cool due to its good thermal contact with water-cooled copper walls. The rectangular elements (W) in a solid boron nitride wall could be raised to about 300°C, but conduction to the cold wall edges prevented achieving higher temperatures. We thermally "floated" the circular disc boron nitride or beryllia insulator (D, Figure 7) in a "Lava" machinable ceramic wall by supporting it only on a circumferential ridge and central point; this gave very poor thermal contact with Lava, which is itself a poor thermal conductor. The tapered disc electrodes were held to the insulator disc, and the disc held to the wall, solely by tension in the thermocouple leads, which also served as probe electrical leads. Stainless steel electrodes were used in all three probes. The removable channel walls bearing probes were cemented to the copper channel with silastic. Calculations of the thermal response of the probe elements indicated that, after a few seconds initial transient, the
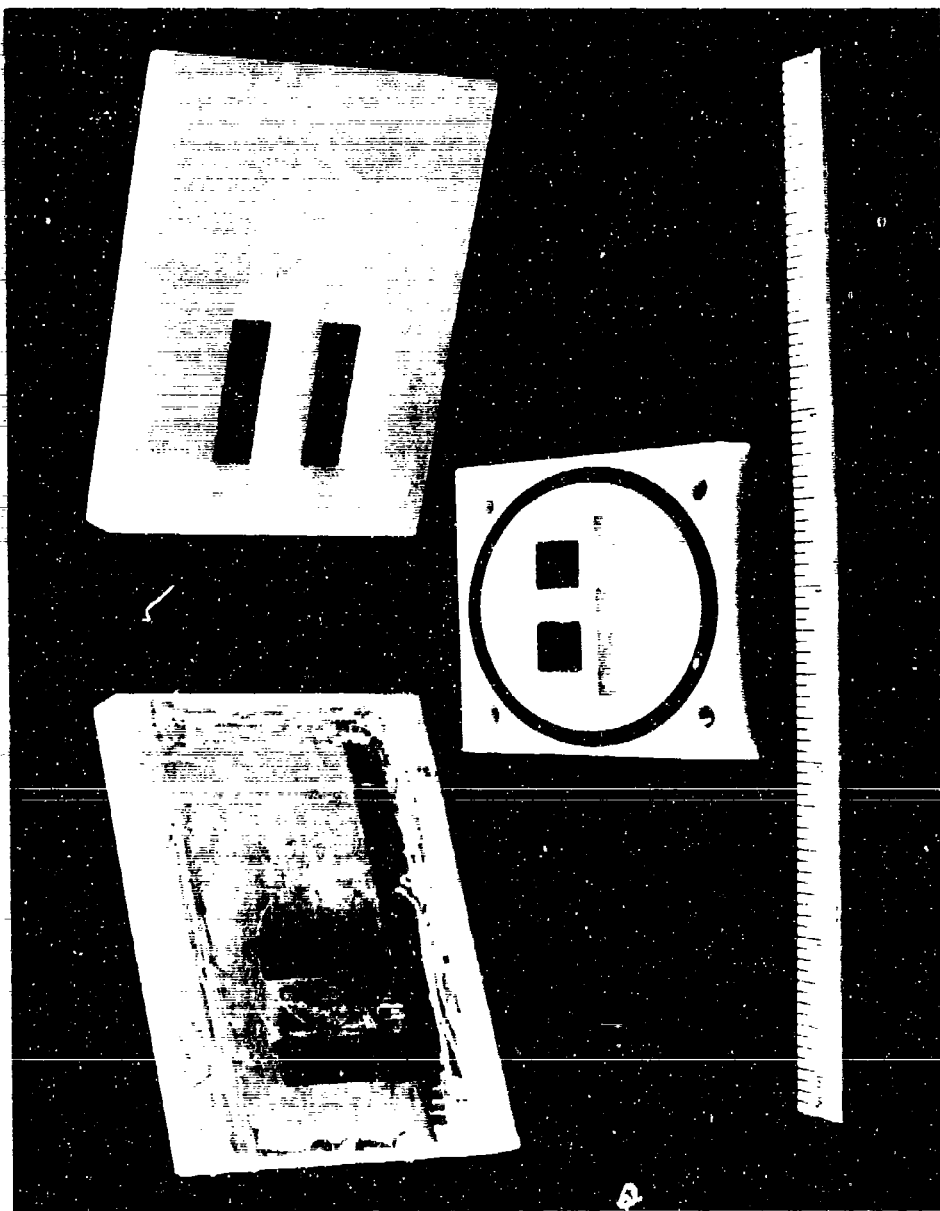
Figure 10. Flush Electrostatic Probes Used in Arc-channel

back face of the solid boron nitride wall achieves a temperature within 10 percent or less of the front face; the stainless discs will track the insulator disc to the same accuracy. The ultimate temperature achieved by the floating disc probe is limited at about $1400°K$ by radiative equilibrium with the aerodynamic heat transfer, with a heat flux of order 4 cal/cm^2-sec at a flow enthalpy of 3000 Btu/lb.
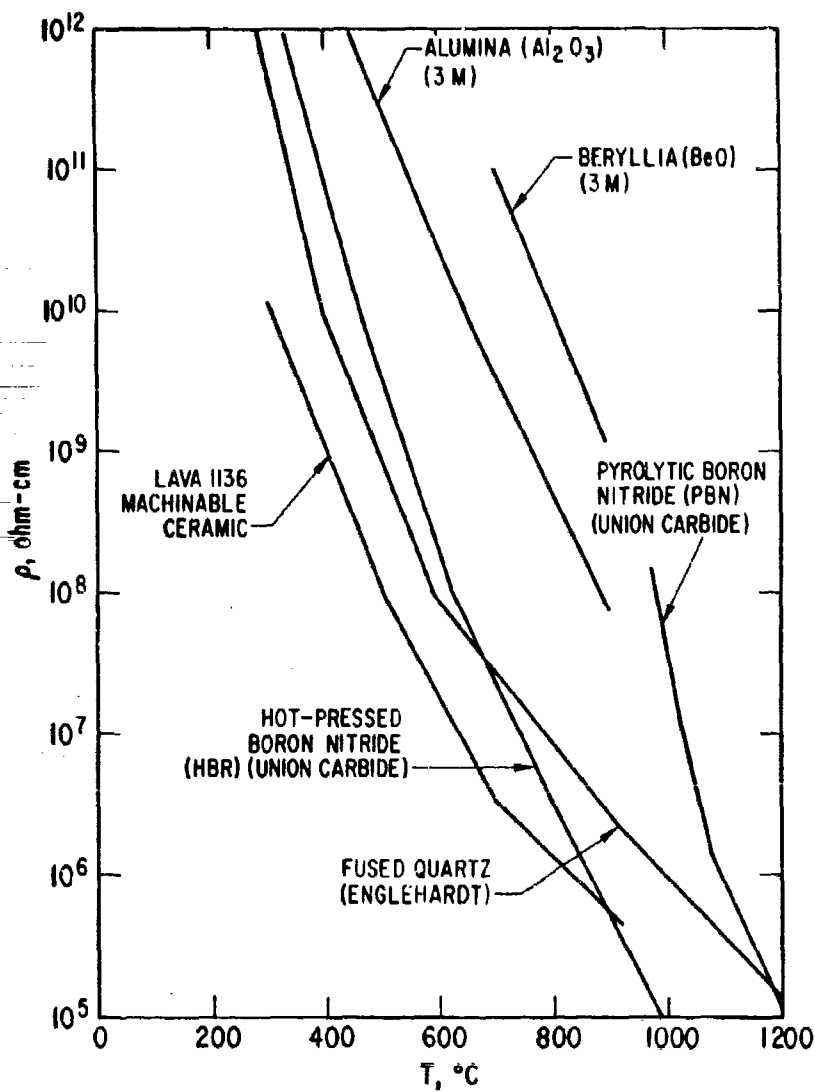
Figure 11. Electrical Resistivity vs Temperature for
High-temperature Insulators

V. HIGH TEMPERATURE MATERIALS

The performance of electrostatic probe materials at high temperature is an important consideration in probe design. Typical probe currents will be of order 10^{-6} amp at 10 v, requiring an insulator resistivity of order 10^8 ohm-cm or better if leakage currents are not to contribute large errors. Resistivity-temperature characteristics of typical candidate insulators are shown in Figure 11. Thermal conductivity and density, specific heat, and thermal diffusion parameter $(\pi K\rho\, C_p)^{1/2}$ are shown in Figures 12-14. Depending upon vehicle and mission requirements, the probe insulator may be required to match heat shield surface temperature and ablation characteristics, or may be permitted to remain cool, so that the materials specifications can be relaxed. For reentry times of 10 sec or less, calculations (Ref. 16) have shown that the insulation slab may be considered semi-infinite, and hence the surface temperature of the various materials will scale as $(\pi K\rho\, C_p)^{-1/2}$. Although beryllia (BeO) is thermally best, its brittleness, poor machinability, extreme toxicity, and poor thermal shock resistance make it unsuitable in general. Boron nitride is the next best choice and is widely available and easily fabricated. In particular, pyrolytic boron nitride has been found to closely match the ablation characteristics of carbon phenolics[3] and will thus maintain structural integrity of the heat shield down to low altitudes. Alumina, the various ceramics, and quartz are thermally poor and are not easily machinable.

Electrode materials must retain structural integrity at high temperature and must not form oxide layers whose electrical resistance can impede ion collection. Copper and tantalum are thus eliminated; molybdenum is almost unmachinable. The 300 series stainless steels have performed well in the present arc tests, and noble metals may also serve.

---

[3]H. DeBolt, AVCO/MSD, private communication.
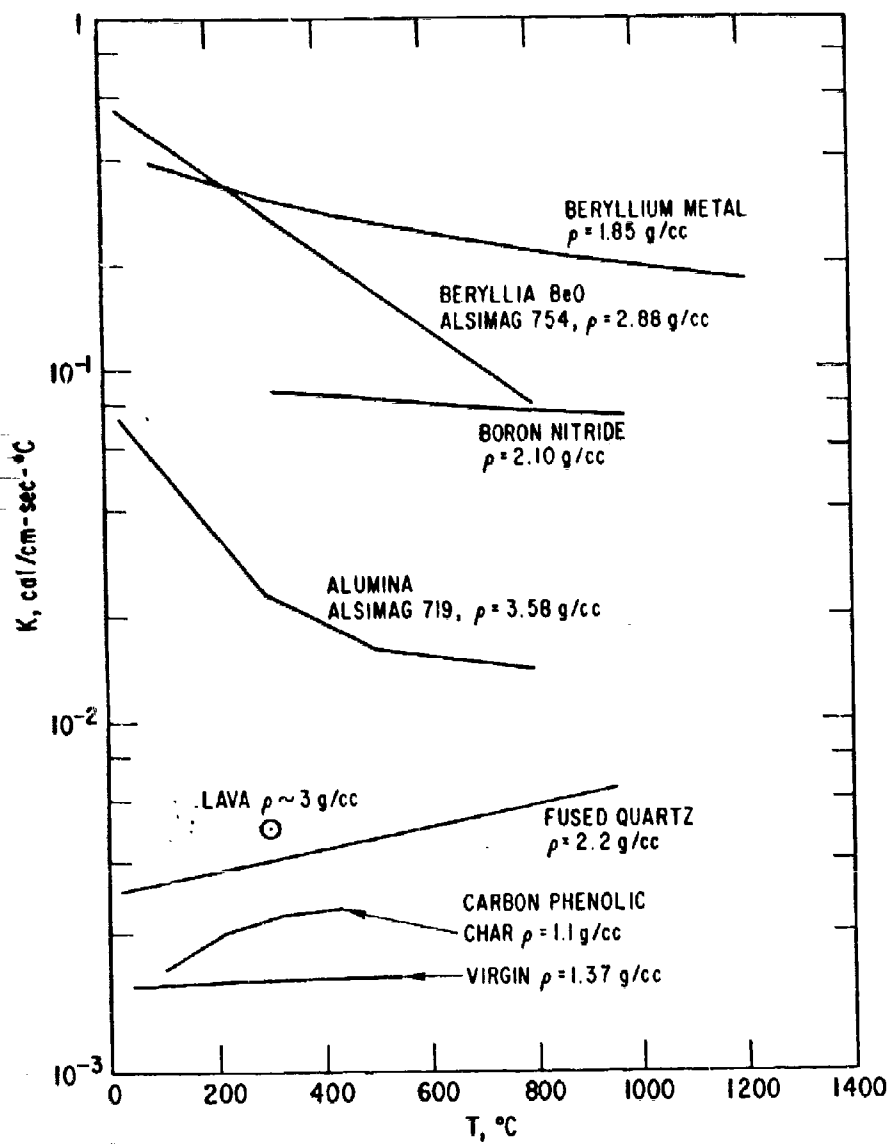
Figure 12. Thermal Conductivity and Density for
Heat Shields and Insulators
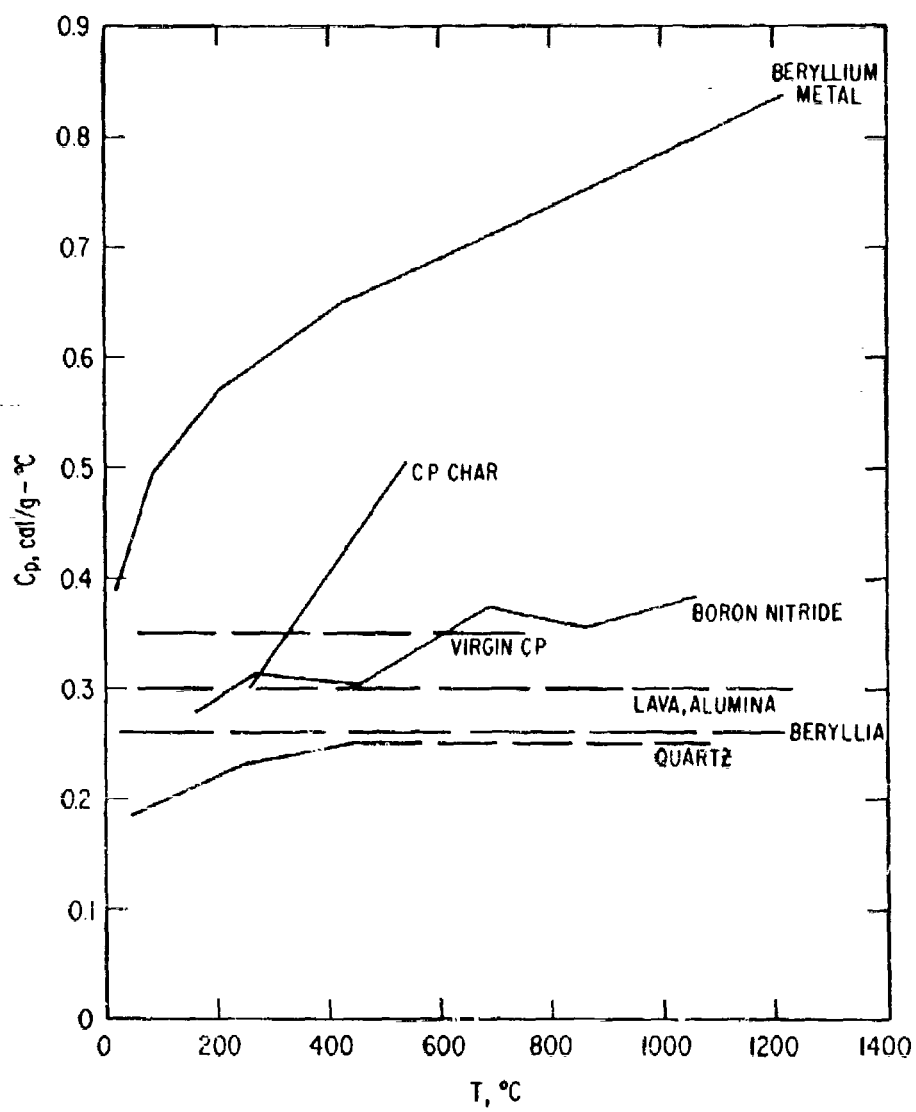
Figure 13. Specific Heat for Heat Shields and Insulators
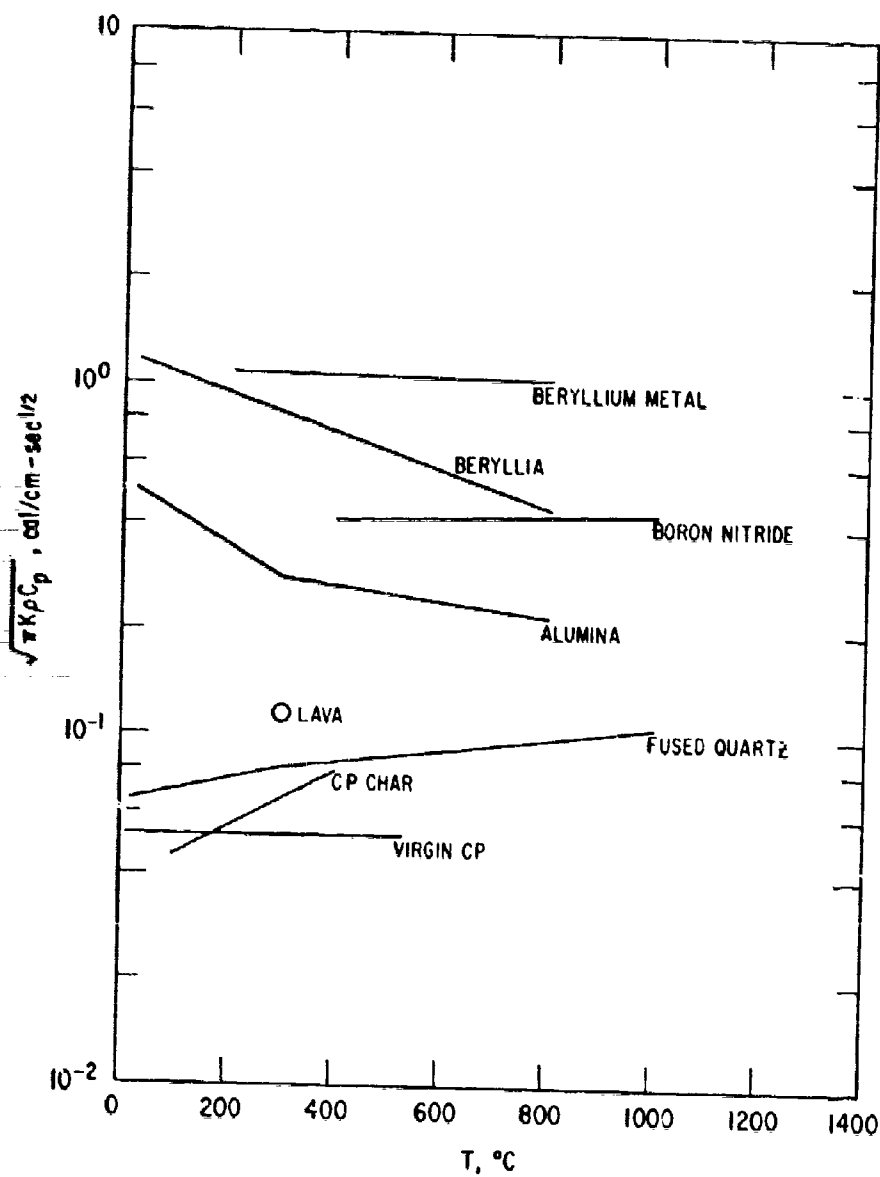
Figure 14. Thermal Parameter $(\pi K \rho C_p)^{1/2}$ for Heat
Shields and Insulators, Scales Temperature in
Semi-infinite Slab under Constant Heat Flux

Chemical contamination of the probe, changing its leakage resistance or current collection characteristics, may occur on ablating vehicles. In order to obtain an estimate of this effect, we have fabricated the probe shown in Figure 15. A strip of carbon phenolic upstream of the probe is permitted to ablate over the probe during a run. Thermal calculations ensure that over a period of 30 sec the sample will have fully charred and begun to recede, so that the full pyrolysis and ablation history is simulated, as confirmed by post-test inspection.
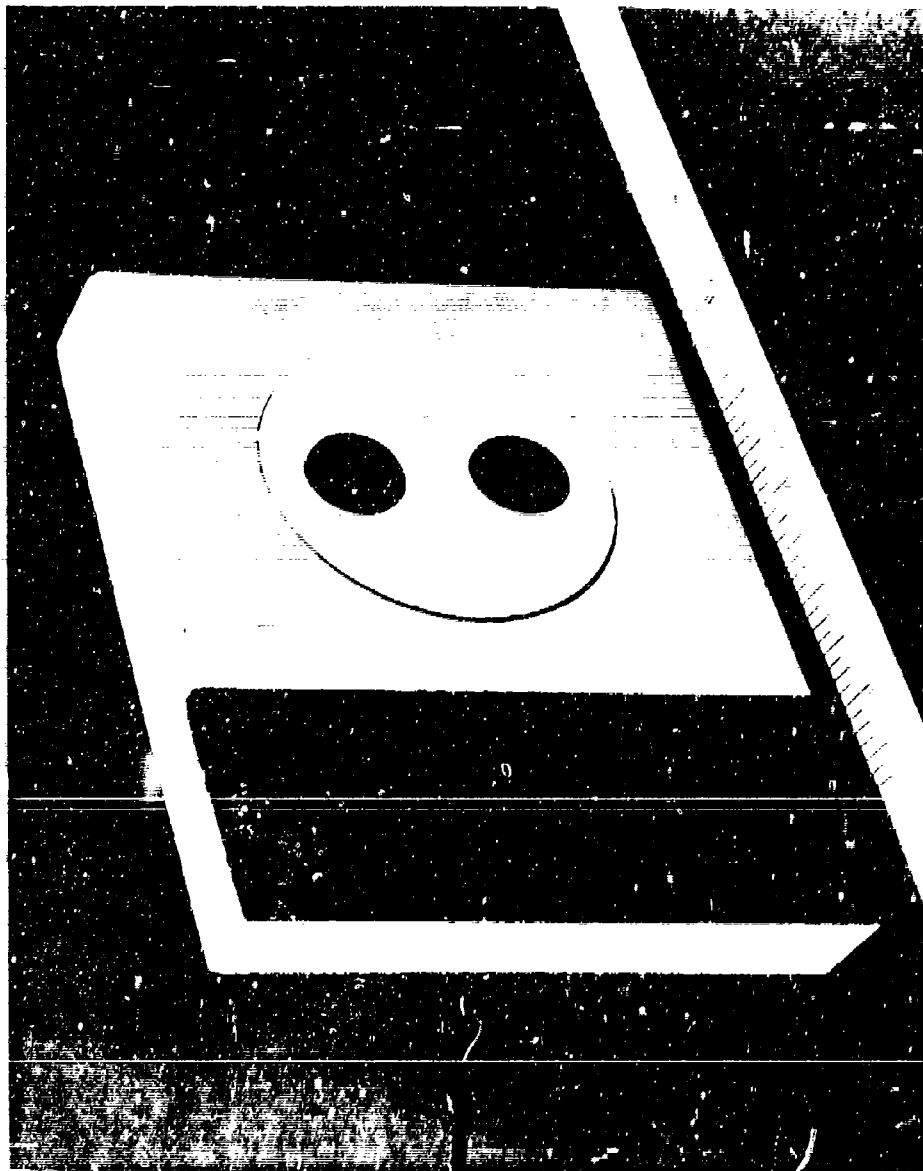
Figure 15. High-temperature Disc Probe with Boron Nitride Insulator in Lava Wall, Stainless Steel Electrodes

VI. PROBE ELECTRICAL CIRCUITRY

Since the arc-channel facility is steady state, and wall temperature variations during tests have a period of many seconds, dc instrumentation was used for the most part. The operating circuit is shown in Figure 16. Either calibrated microammeters or a stripchart recorder were used for measurement of probe current and thermocouple voltage. The V-I characteristics of the probe were plotted stepwise by switching voltage and recorder polarity. Oscillographic recording introduced serious noise and ground loop problems from the arc, and inevitable high frequency arc fluctuations made accurate data interpretation difficult. Rapid sweeping of the probe and determination of electron temperature were not successful. This confirmed earlier work in arc-jet flows (Ref. 6) that showed that time-dependent contamination effects prevent meaningful or reproducible electron collection at high currents unless special techniques of probe cleaning and fast voltage sweeping are employed, which could not be done in the present work. Surface resistance and voltage drop are negligible in the ion saturation regime since current density is low, but it becomes a serious problem at high electron currents. In addition, since the probe is operating in a highly nonuniform boundary layer, the sheath position, local n_e at the sheath edge, and collected current density will all change with bias voltage and will reflect the flow profile as well as the electron temperature. However, the probe floating potential (V_b when $I = 0$) can be determined by sweeping, and we must determine it to ensure that negative bias voltages are sufficient to reach the ion saturation regime desired.

Mode switching permits operation of the probe in three electrical configurations: D, floating double probe; R, single element probe (other element grounded to copper channel walls); or S, both electrodes shorted together to form a single probe of twice the area (to check on geometry and sheath area corrections with voltage again referenced to channel walls).

ELECTRODES
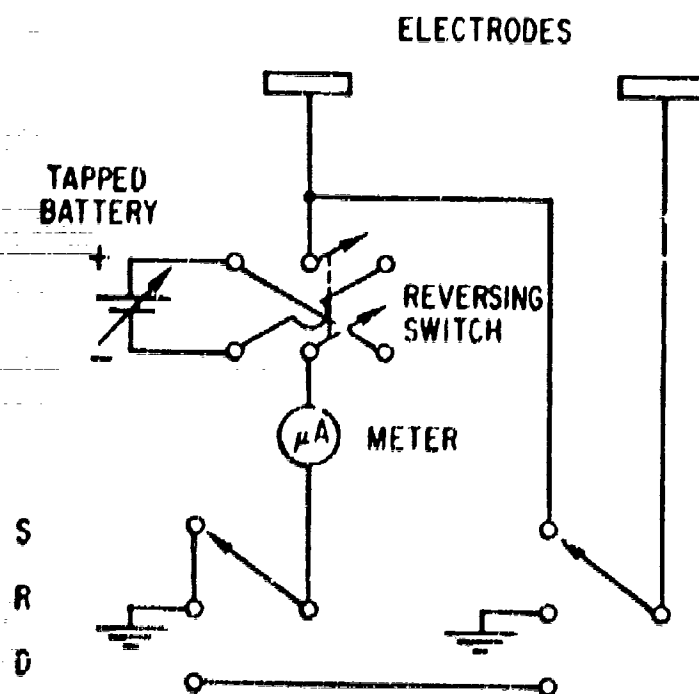
Figure 16. Electrical Circuits for Flush Probe Tests in Arc-channel

VII. FLUSH PROBE THEORY OF OPERATION

Two different theoretical models of flush probe operation in a boundary layer are considered. In ion saturation, Bredfeldt et al. at Stanford Research Institute (SRI) (Ref. 1) suggest a model of the collison-dominated sheath on a planar probe and assume that all the random thermal drift current of ions at this sheath edge is collected by the probe. The B. L. fluid dynamics is a separate input, and serves only to establish the n_e profile so that n_s at the sheath edge can be calculated. Chung and Blankenship (Ref. 2) have simplified Chung's earlier analyses (Refs. 17 and 18) for the case of ion saturation operation under conditions where the sheath is very thin compared to the fluid boundary layer. When hypersonic approximations are used, the current collected by the probe is dependent only on the fluid dynamics; the probe serves only to establish boundary conditions for n_e. Both theories have failings. In the case of the SRI theory, the fluid dynamic velocity and electron density profiles must be known in detail, which is unhandy for flight test analysis. Chung's case depends only on the peak n_e and on good engineering approximations for the boundary layer structure and electrical behavior. However, no dependence of current on probe bias is predicted. Both theories require assumption of the ion Schmidt number or mobility, which is not at all clearly established for a highly nonuniform boundary layer.

The details of the SRI theory for both cylindrical and planar probes are summarized in Refs. 1, 19, and 20. We restrict our discussion to bias voltages sufficiently negative that the probe draws ion saturation current J. The mobility-controlled sheath thickness d_s on a planar electrode is given by

$$J = \frac{n_s \, e \, v_{th}}{4} = \frac{1}{A} \qquad \text{ion drift saturation current per unit sheath area at sheath edge} \qquad (1)$$

$$= \frac{9 \, \epsilon_o \, K_i \, V^2}{8 d_s^3} \cdot \qquad \text{mobility-limited sheath (Ref. 15)} \qquad (2)$$
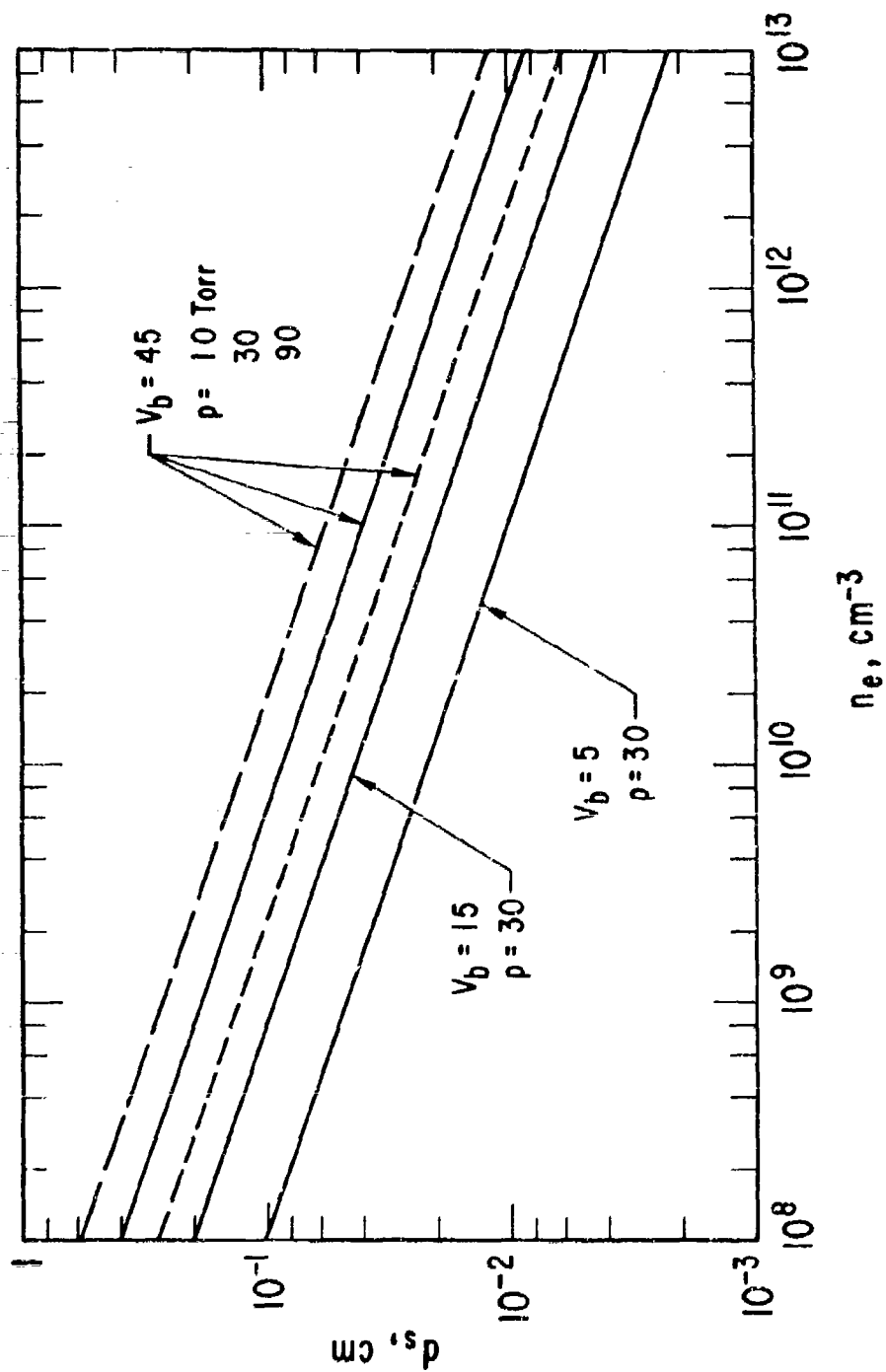
Figure 17. Ion Sheath Thickness as a Function of Bias Voltage and Electron Density at Sheath Edge

-28-

where n_s is electron (= ion) density at the sheath edge, v_{th} is ion thermal velocity, e the electron charge (singly charged ions assumed), ϵ_o the permittivity of free space, K_i the ion mobility, and V the probe potential with respect to the plasma. The ion mobility is given by (Ref. 21)

$$K_i = \frac{e}{m_i \nu_m} \frac{e}{Q_m n_g v_{th}} \tag{3}$$

where n_g is neutral gas number density, m_i is ion mass, and Q_m and ν_m the momentum transfer cross section and collision frequency. In reality, the mobility will vary through the sheath as a function of field strength, density, and temperature. However, the 1/3 power dependence of d_s on K_i permits the approximation of constant K_i. We assume (Ref. 1) that all ions in air are NO^+ and $Q_m = 1.3 \times 10^{-14}$ cm^2, $m_i = 5.01 \times 10^{-23}$ g. We also note that

$$v_{th} = \left[\frac{8\, kT}{\pi\, m_i} \right]^{1/2} \tag{4}$$

where we assume $T_g = T_i = T_e$ at the boundary layer peak temperature and k is Boltzmann's constant, 1.38×10^{-16} erg/°K. Then the sheath thickness is given by

$$d_s = \left[\frac{9\, \epsilon_o\, e}{8\, Q_m\, m_i\, n_g\, v_{th}} \right]^{1/3} \left[v_b + 5kT/e \right]^{2/3} \left[J \right]^{-1/3}$$

where the term $5kT/e$ represents the Langmuir (floating) potential. We shall always operate in ion saturation where $V_b \gg 5kT/e$. Sheath thickness as a function of n_e and V_b is plotted in Figure 17. (Note that since $n_g \sim p/T$, d_s is independent of T at constant p and is also independent of ion mass if Eqs. (1) and (4) are used for J.) When the sheath thickness is an appreciable

fraction of the probe dimension, corrections for sheath edge area must be made to A; simply multiplying the perimeter by d_s is equivalent to the SRI use of a 60-deg segment of the cylindrical edge. Convection of ions into the upstream edge of the probe sheath is non-negligible at hypersonic velocities, but can be ignored in the subsonic channel flow. The correctness of Eq. (1) for a collision-dominated sheath and the true effects of combined convection and diffusion as a function of sheath thickness and probe size are not satisfactorily established at present. On the basis of results taken from Ref. 1 and presented in Figures 18 and 19, the correlation between cylindrical wire probes and flush probes in probing the boundary layer n_e profile is excellent. And, on the basis of comparisons with microwave measurement, the flush probe theory with semiempirical corrections (Ref. 1) seems good to a factor of 2 to 4 in determining absolute electron density. Since the boundary layer profile in the SRI shock tube experiments duplicates qualitatively the temperature at peak n_e, the thickness δ, and hence the ion transport properties appropriate to conical vehicle reentry, the theory appears to be adequately tested and proven within the limits inherent in the assumptions and the experiment. The assumptions of chemical freezing and thin sheath limit the applications to $10^{12} > n_e > 10^9$. In practical use, the measured probe current I and the geometric area A are used to find J. If T_s and v_{th} are known from the assumed B. L. structure, Eq. (1) yields n_i, whence, using V_b, Eq. (5) yields d_s. Small corrections for sheath edge area and convection (assuming the u profile is known) are then made to yield final values of n_i at d_s.

Chung's analysis (Ref. 2) requires several basic assumptions. The sheath must be much thinner than the shear layer; this requires

$$10^3 < \hat{A} = \frac{\hat{\Delta}^2 e^2 n_{eo}}{\epsilon_o kT_\delta} = \left(\frac{\hat{\Delta}}{\Lambda}\right)^2; \qquad \Lambda = 6.9\left(\frac{T_\delta}{n_{eo}}\right)^{1/2} \qquad (6)$$
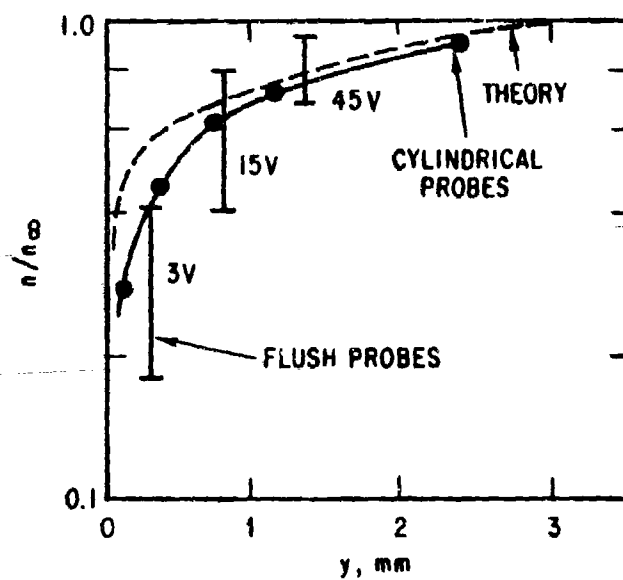
Figure 18. Comparison of Theoretical
Electron Density Profile in a Shock
Tube Flat Plate Boundary Layer
with Cylindrical and Flush
Electrostatic Probe
Measurements
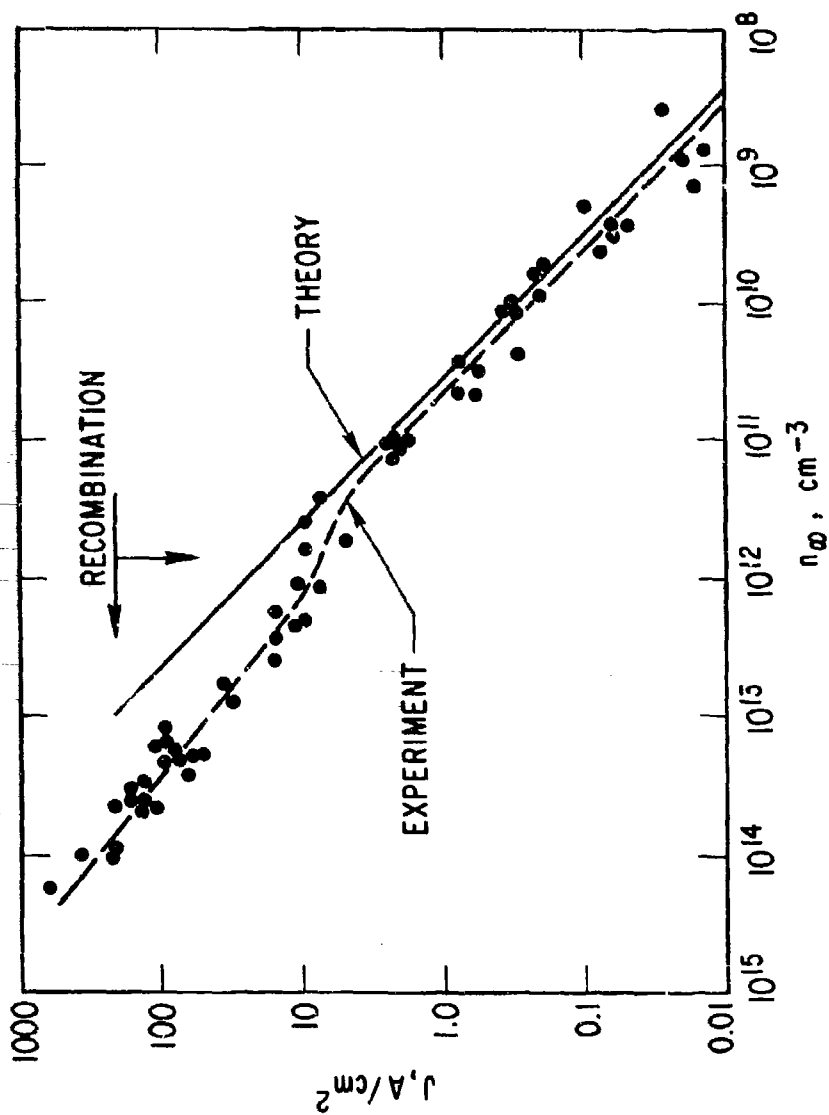
Figure 19. Comparison of Predicted and Measured Ion Currents in
a Shock Tube Flat Plate Boundary Layer using Flush Probes

where n_{eo} is the peak electron density in the boundary layer, T_δ is the freestream temperature at $y = \delta$, the boundary layer edge, Λ is the Debye length, and

$$\hat{\Delta} = \int_0^{y_o} \rho/\rho_o \, dy \qquad (7)$$

is essentially a boundary layer displacement thickness. Subscript o refers to the temperature (or n_e) peak, and δ to the outer edge, of the boundary layer. It is assumed that phenomena are essentially controlled by the highly conductive layer about y_o, T_o, n_{eo}. The similarity parameter η is given by

$$\eta = \left[\frac{3u_\delta}{2 \, l \, \rho_\delta \mu_\delta x} \right]^{1/2} \int_0^y \rho \, dy \qquad (8)$$

where u is flow velocity, ρ and μ are density and viscosity, and l is the Chapman-Rubesin parameter $(\rho_w \mu_w / \rho_o \mu_o)^{0.2}$.

The ion Schmidt number $Sc_i = \mu/\rho D_i$ is not specified. From simple kinetic theory, $\mu = 1/2 \, \rho L v_{th}$, $D = 1/3 \, L \, v_{th}$, and $Sc = 3/2$ if ions diffuse like molecules. Chung (Ref. 22) has recently correlated his results of Refs. 17 and 18 to show explicitly the effect of varying Sc_i. Comparison with Hoppman's results (Ref. 23) for the parallel plate probe geometry of Ref. 18 shows a best fit to theory with $Sc_i = 1.3$. For the present experiments $Sc_i = 1$ has been assumed and provides adequate fit to the data. Experimental values of ion diffusion or mobility coefficients in air vary widely. Cobine (Ref. 15) suggests values of D_i of order 0.028 cm^2/sec at NTP. Frohn and DeBoer (Ref. 24) suggest mobility of $Kp = 2 \times 10^4 \, cm^2$ torr/v sec for freshly formed NO^+ ions in air at 3000°K with ambipolar diffusion. If we assume the Einstein relation $D\rho/Kp = kT/e$, then $D_i \approx 5 \times 10^3$ at 10^{-3} standard density. Since $\mu \sim 10^{-3}$ at peak boundary layer temperature, this yields $Sc_i \sim 0.1$ if T = 3000°K, but values perhaps an order of magnitude larger at 300°K. The ion temperature is assumed to be in equilibrium with the neutrals throughout the boundary

layer. The clear definition of Sc_i deserves further study for nonuniform flows.

The ion saturation current collected is then given by

$$n_{eo} = \frac{j_{is} Sc_i \rho_o \hat{\Delta}}{2.68 \, \ell \mu_o} \qquad (9)$$

where j_{is} is particle flux of ions/cm^2 sec. Chung (Ref. 2) further extends this result to the highly cooled boundary layer on cones, where

$$n_{eo} = \frac{J \eta_o (Re/\ell)^{1/2} \rho_o \mu_\delta Sc_i (1.9 \times 10^{18})}{\rho_\delta \mu_o u_\delta} \qquad (10)$$

where n_{eo} is e/cm^3, J is in amp/cm^2, and $Re = \rho_\delta u_\delta x / \mu_\delta$. For highly cooled cones, Eq. (19) and Figure 3 of Ref. 2 show that $\eta_o \approx 1.1$.

Several further assumptions are made when these formulae are used in data reduction. For the arc-channel, Eq. (9) is used with $\hat{\Delta} = 0.845$, as calculated from Figure 10. Values of μ were taken from Baulknight (Ref. 25). We measure $\overline{T}$ and p for each arc run and assume that $T_{peak} = 1.5 \, \overline{T}$ and that $p = \rho RT$ for simplicity. The parameter ℓ is of order 1.12, and, as discussed earlier, we arbitrarily set $Sc_i = 1$. Then

$$n_{eo} \, (cm^{-3}) = \frac{1.01 \times 10^{15} \, p(torr)}{\mu_o (poise) \, T_o (^\circ K)} \, J(amp/cm^2) \qquad (12)$$

For flight estimates, Eq. (10) is used directly, and the boundary layer structure is as specified in Figures 4, 5, and 6, with $\eta_o = 1.1$.

Chung (Refs. 1, 17, and 18) has considered the limitations of this theory and finds that for the requirements of frozen recombination and $\hat{A} > 10^3$ we must have $10^{11} < n_e < 10^{15}$ for reasonable temperatures and

pressures achieved in laboratory or flight. In the shock tube, Bredfeldt et al. (Ref. 1) found recombination to be serious for $n_e > 10^{12}$. Calculations of $\bar{A}$ show that $\bar{A} < 10^3$ for $n_e \lesssim 10^{10}$, so it appears that in flight the most serious limitation is in the thickening of the sheath at low n_e. For the arc-channel tests, $\hat{A} \sim 10^4$ and $10^{11} < n_e < 10^{13}$, so that the theory should apply. We also assume implicitly throughout that ion and electron temperatures are equal to neutral temperature at the channel centerline, but that T_e remains frozen at the centerline value throughout the flow.
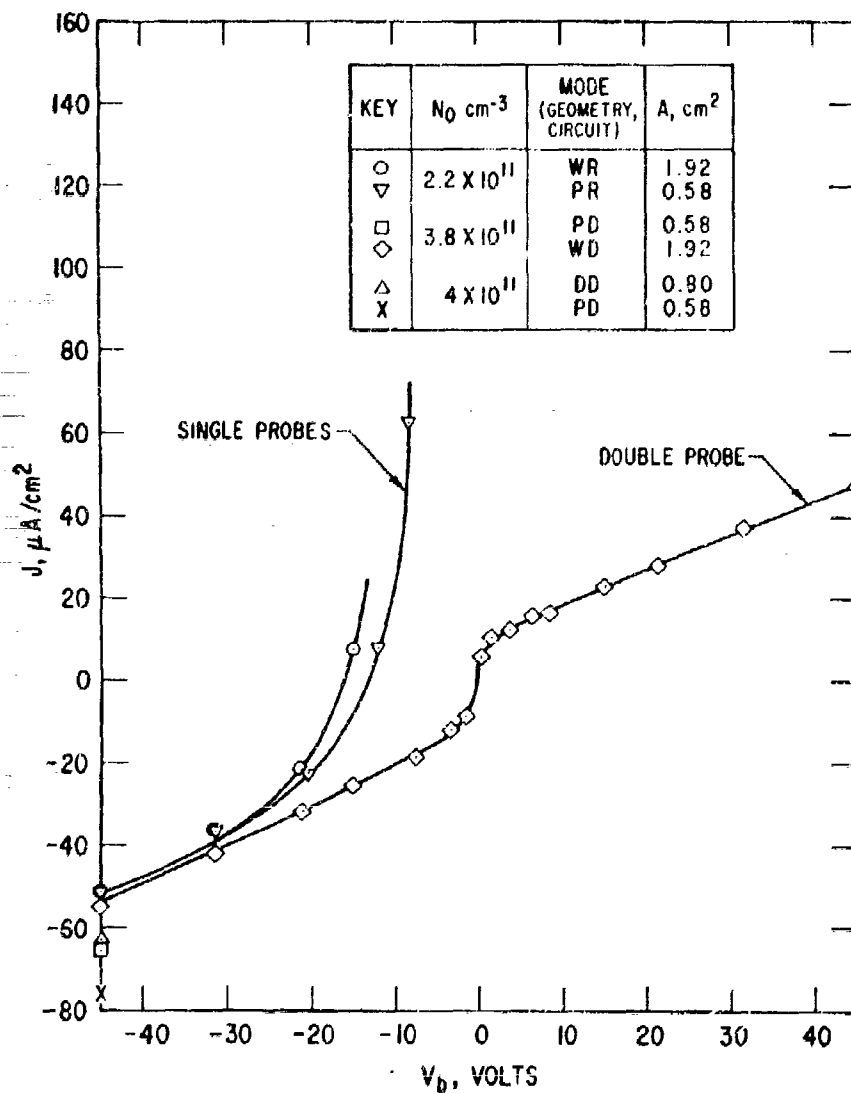
Figure 20. Current - Voltage Characteristics of Three
Probe Configuration

VIII. EXPERIMENTAL RESULTS

A. GENERAL OPERATION

The program of runs was designed to establish the effects of varying the following parameters: probe geometry (plug, wall, or disc); probe mode (single probes with reference electrode grounded, or both electrodes shorted together, or floating double probe); insulator material; surface temperature; carbon phenolic ablation; and ambient n_e and to establish the correlation between the microwave measurement of n_e and the probe collected $J_{i_{sat}}$ through the Chung and SRI models. Over 50 runs were taken, covering a range of n_e from 2×10^{11} to 3×10^{12}, with various probes singly and in combination. Only a portion of the data is presented to illustrate the major conclusions drawn.

Figure 20 presents several V-I characteristics at the lower electron densities. It was found that for a single probe the floating potential (i.e., V_b when $I = 0$) is -15 ± 2 at $n_e = 4 \times 10^{11}$ and -5 ± 1 at $n_e = 3 \times 10^{12}$. No attempt was made to interpret electron currents for reasons discussed earlier. The floating double probe shows an appropriately symmetric characteristic. By comparing ion saturation current for the three probe configurations, we reached the following conclusions:

1. J at $V_b = -45$ is independent of the choice of probe geometry or circuitry, varying less than ± 15 percent for the three configurations tested.

2. There is no interaction of two probes, e.g., the plug and wall types, when they are placed directly opposite each other. Although the electron sheaths on the negative electrodes are as thick as the channel, their interaction does not affect probe performance.

3. Corrections for convection and sheath area made according to the SRI theory require a reduction in J (based on geometric area of the probe) of no more than 30 percent.

-37-
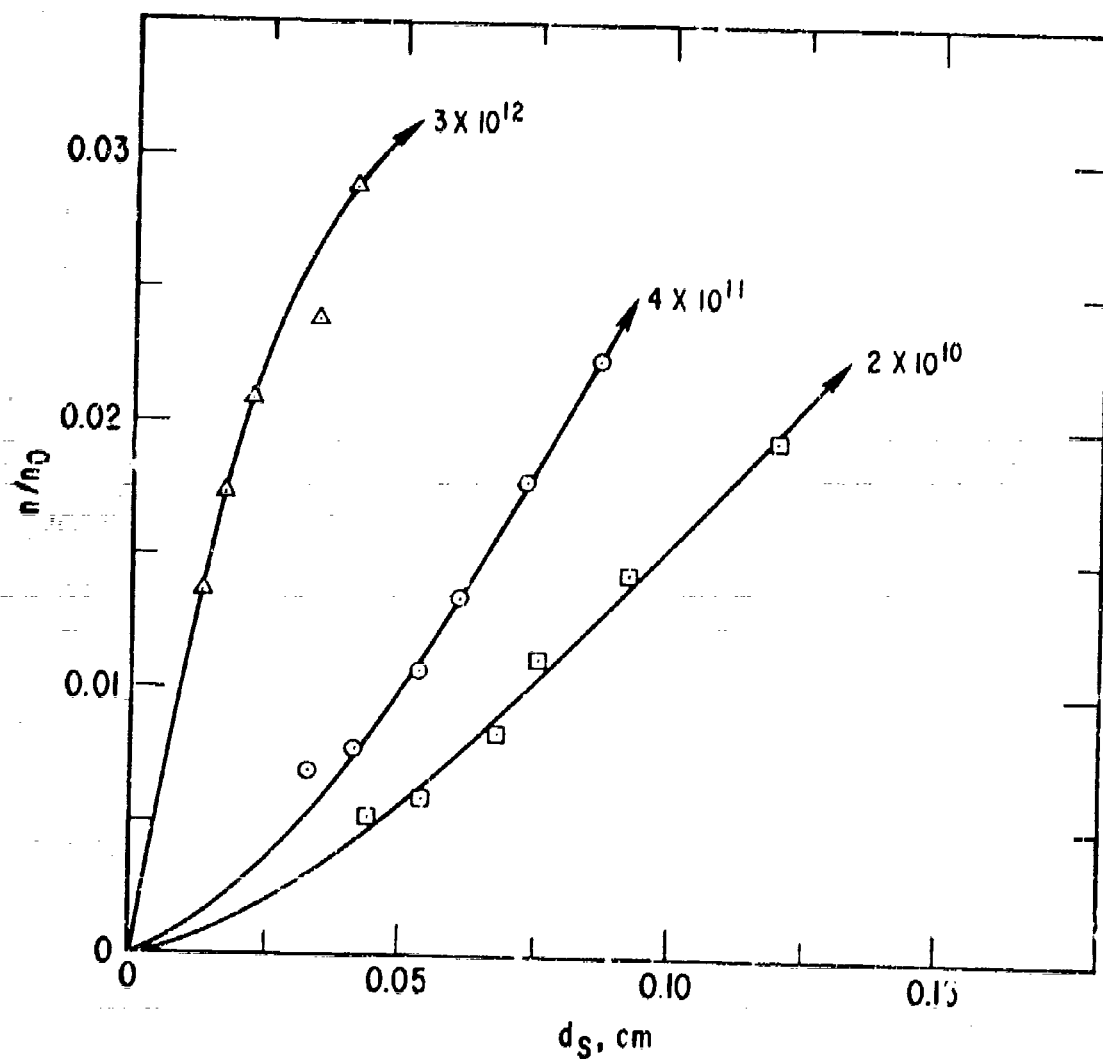
Figure 21. Ion Density Profiles in Arc-channel from Flush
Probe Measurements

Recent experimental and theoretical studies[4,5] of the effects of sampling the boundary layer profile by varying probe voltage have shown that the current density is a function of probe length in the flow direction. Since all of our configurations have comparable streamwise size and since the electrodes are electrically independent, being separated by several sheath thicknesses, these effects were not observed.

For data reduction with the SRI model, it was initially assumed that $T = 3000°K$ and $v_{th} = 1.45 \times 10^5$ cm/sec. Then Eq. (1) yields n_s at the sheath edge and Eq. (5) and Figure 19 provide the sheath thickness d_s (which varies with V_b as we sweep through the probe characteristic). These values are plotted in Figure 21, normalized to the peak n_e, for several runs. Several conclusions are immediately apparent:

1. The measured n_e profiles fall far below the assumed profile obtained by extrapolating the 3-point rake measurement to the wall (cf. Figure 8).

2. The curvature reversal between high n_e, high pressure and low n_e, low pressure cases is very clear and reproducible. Although no detailed theoretical model is available, these observations are consistent with a strong depletion of n_e near the wall by diffusion and surface recombination. The discrepancy is far outside any possible error in the approximate data reduction method used; detailed iteration on n_e, d_s, T_s and v_s profiles does not appreciably change the resultant measured n_e profile. Thus it appears that we cannot employ this experiment to verify the SRI theory, since we apparently do not know the profile near the wall a priori. The SRI calibrations of Figures 18 and 19 serve to establish the validity of their approach.

Table 1 summarizes all runs for which microwave data are available. Results of data reduction based on the Chung theory [Eq. (11)] and SRI model, with approximate sheath area and convection corrections, are shown. These data are plotted on the basis of Chung's theory in Figure 22, where n_{e0} predicted from Eq. (11) is compared to the microwave measurement. The microwave measurement is accurate to about ±30 percent. Although Chung's theory does not explicitly consider any detailed mechanism of current

---

[4] R. Keil, Bell Telephone Laboratories, private communication.

[5] W. Schaifman, Stanford Research Institute, private communication.

Table 1. Comparison of Microwave Measurements of n_e with Flush
Probe Results Using Chung and SRI Theories
($V_b = -45$, ion saturation)

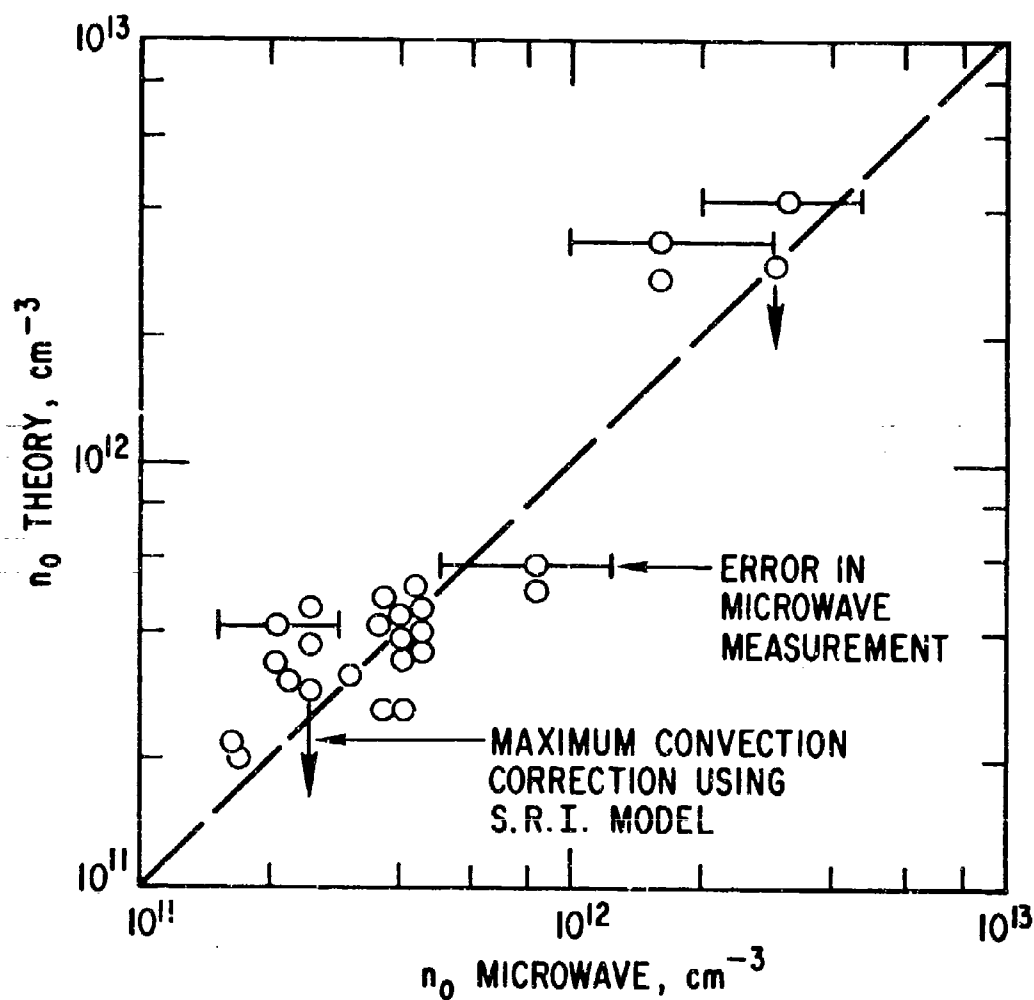| Run	Mode V_b - 45 (see Fig. 18)	n_o Microwave, cm^{-3} × 10^{11}	A, cm^2 10^{-5}	J, A/cm^2 × 10^{11}	p, torr	T_o, °K	n(Chung) Eq. (9), cm^{-3} × 10^{11}	n(SRI) Eq. (1), cm^{-3} × 10^9	d_s, cm
				Data				Results	
7-22-2	WR	4.02	1.93	5.09	30	4150	3.58	8.8	0.09
	PR		0.58	5.18			3.64	8.95	0.09
-3	WR	3.90	1.93	3.74	30	4150	2.63	6.47	0.097
-4	WD	4.02	1.93	6.21	30	4150	4.36	10.7	0.082
	PD		0.58	6.41			4.51	11.1	0.081
-5	WD	4.02	1.93	6.21	30	4150	4.36	10.7	0.082
-6	WS	3.78	3.86	3.63	30	4150	2.55	6.29	0.098
	PS		1.16	3.70			2.60	6.4	0.099
7-25-1	WR	4.3	1.93	5.7	30	4150	4.0	9.86	0.085
	PR	6.7	0.58	6.7			4.71	11.6	0.081
	WD		1.93	7.0			4.92	12.1	0.079
	PD		0.58	5.2			3.66	8.95	0.088
-2	WR	3.06	1.93	4.5	30	4150	3.16	7.35	0.093
	PR		0.58	4.5			3.16	7.76	0.092
-3	WD	3.76	1.93	6.21	30	4150	4.37	-	-
	PD		0.58	6.55			4.61	-	-
8-9-1	WD	8.3	1.93	8.0	28	4150	5.63	13.8	0.076
	PD		0.58	6.9			4.85	11.9	0.079
-2	WD	15.2	1.93	60	30	4800	33.2	10.2	0.037
7-22-9	WR	2.2	0.58	5.19	16	3500	3.0	8.96	0.114
-10	WS	1.68	3.86	3.63	16	3500	2.1	6.28	0.104
	PS		1.16	3.7			2.19	6.56	0.103
8-9-3	WD	3.1	1.93	72.5	40	5600	41.6	125	0.036
7-25-5	WR	2.02	1.93	2.48	41	3000	4.01	-	-
	PR		0.58	2.06			3.35	-	-
-6	WD	2.42	1.93	2.70	41	3000	4.40	4.67	0.10
	PD		0.58	2.28			3.70	-	-
	PR		1.93	2.3			3.74	-	-
	PS		1.16	1.73			2.82	-	-
8-11-3	DD	15.2	0.80	50	30	4800	27.7	86.5	0.042
-2	DD	4.0	0.80	6.25	30	4150	4.4	10.8	0.08
-4	DD	30	0.80	52.5	40	5600	30	91	0.04
8-26-1	BeO WR	30	1.93	53	40	5600	30	91	0.04

Figure 22. Arc-channel Electron Density Using Chung Theory
Compared to Microwave Measurement
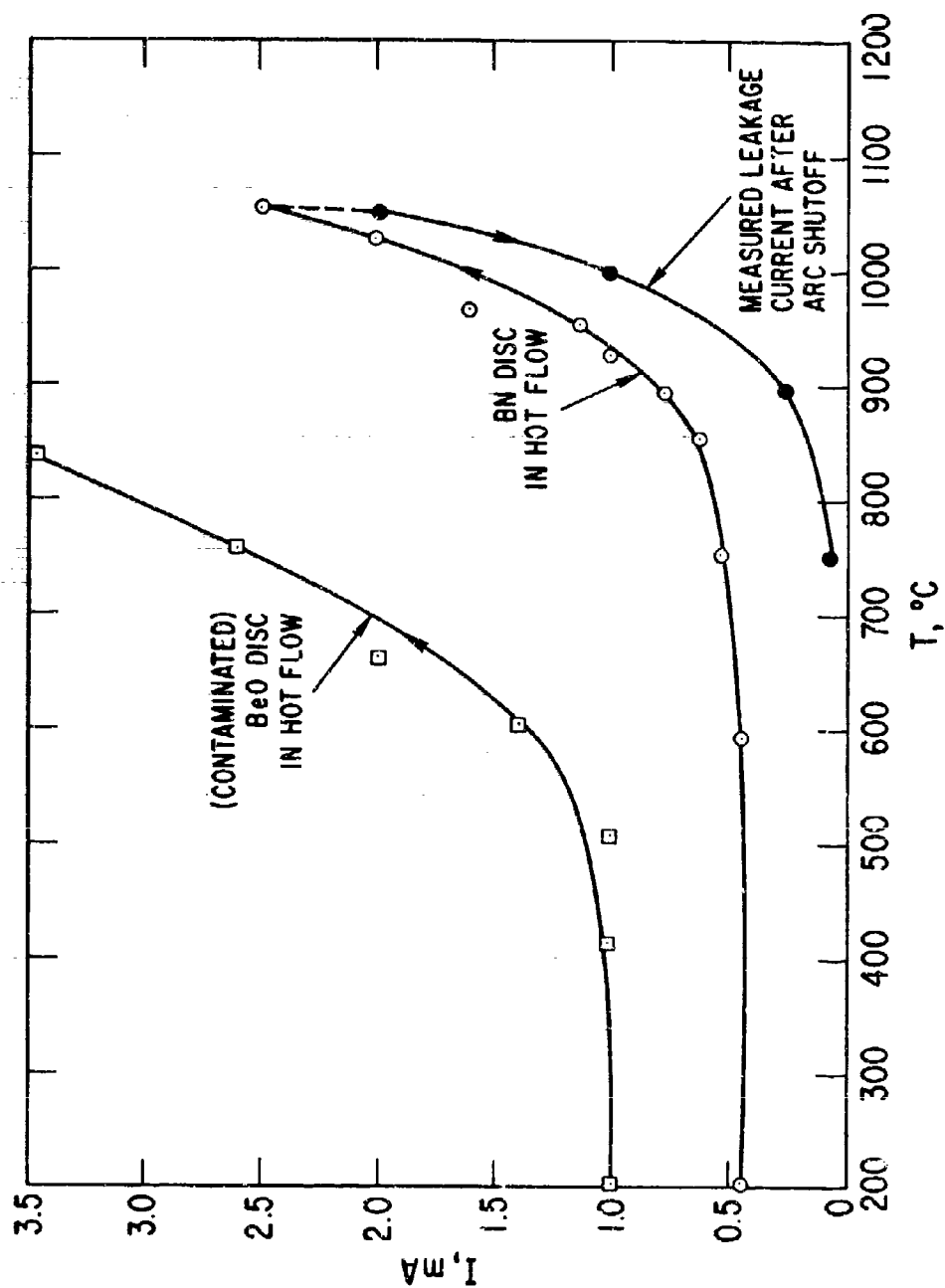
Figure 23. Probe Current as a Function of Insulator Temperature, Showing
High-temperature Ohmic Leakage, Disc Probe

-42-

collection, the magnitude of correction to J, and hence to n_{eo}, for convection sheath area effects in the SRI model is shown. All of the data fall within a factor 2 of the microwave measurement, with a mean deviation of ± 25 percent. It is concluded that, within the accuracy of the experiment, Chung's theory will accurately predict peak n_{eo}, with $Sc_i = 1$, and that this theory can be reliably used for the evaluation of flight measurements within the range of validity as discussed earlier.

B. HIGH TEMPERATURE EFFECTS

The foregoing measurements and conclusions are valid up to surface temperatures of about 800°C with stainless steel electrodes in a boron nitride insulation. With the solid boron nitride channel wall, we were never able to exceed 320°C. With the thermally floating disc probe, however, we achieved temperatures up to 1020°C, and it is in the region above 800°C that anomalous probe behavior is observed.

A typical run made with the disc probe is plotted in Figure 23. The surface temperature of the stainless steel electrode was indicated by the embedded Cr-Al thermocouple. Since the test duration was about 80 sec, with a steady T_w rise of 10°/sec up to 1000°C, good thermal equilibration of the probe elements was predicted from heat transfer calculations. The maximum temperature achieved in runs of 2-min duration at maximum channel enthalpy was 1100°C.

The collected probe current was observed to rise steeply above 800°C and to decay over a period of several seconds after the arc shut off. Four repeated runs were made, and the curve was found to be quite reproducible within the errors of temperature - current synchronization. (Temperature and current could not be recorded simultaneously in floating double probe mode since the thermocouple leads served both purposes; hence, the data scatter and synchronization problem were due to switching transients in the recorder and the rapid time rate of current change toward the high temperature end of a run.) One thermocouple was fed to a calibrated microammeter
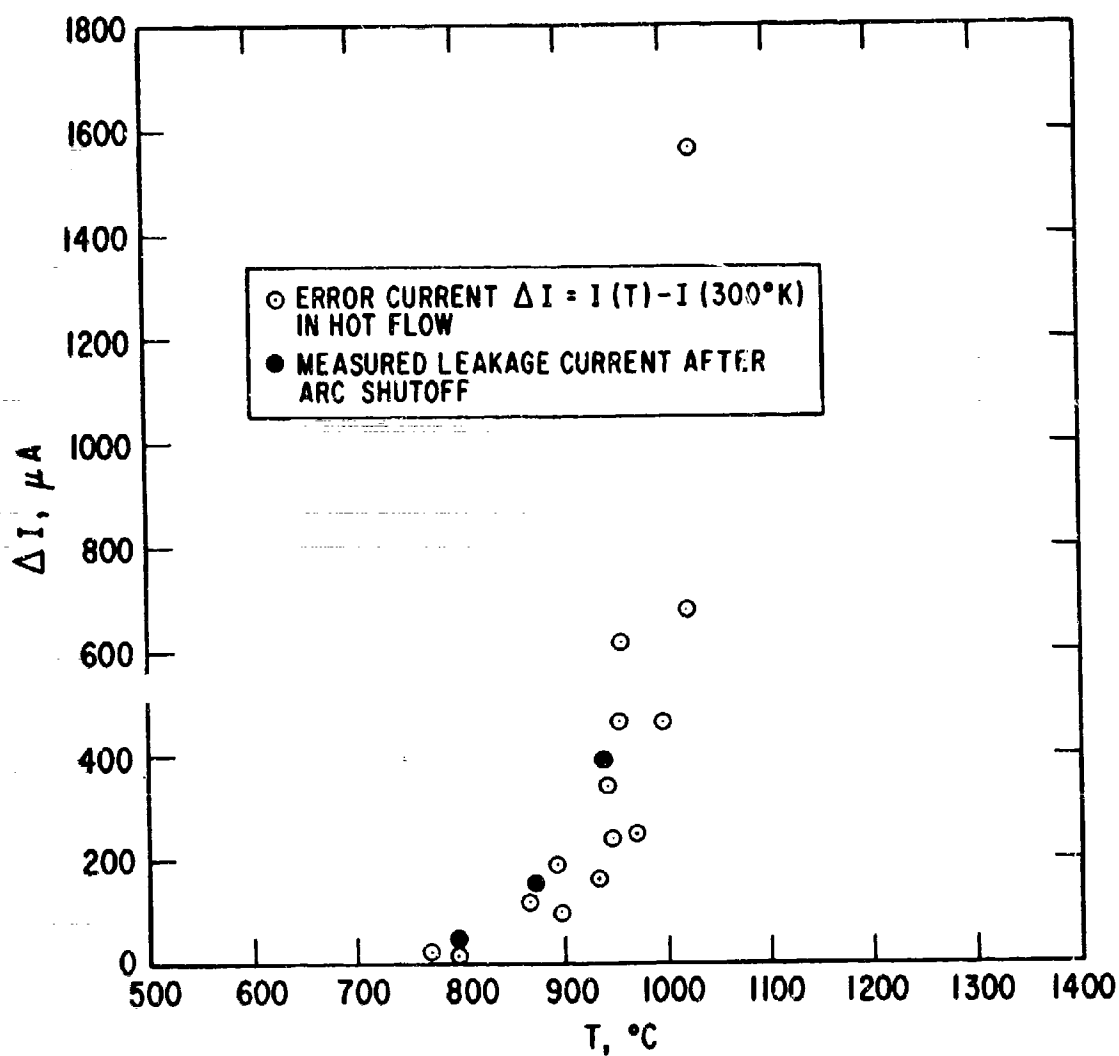
Figure 24. Probe Error Current as a Function of Wall
Temperature, Disc Probe

reading directly in temperature; the other, used for data reduction, was fed to the stripchart recorder. The two thermocouples always agreed within 50°C.

The plug probe was monitored continuously throughout these runs and maintained a constant current. Hence the high-temperature probe current changes do not reflect any variation in the channel flow. The "error current" $\Delta I = I(T) - I(300°)$ for four runs is plotted as a function of temperature in Figure 24. Note particularly that the solid points, representing error current decay after arc shutoff, fall among those obtained during hot flow. All were obtained with double probe at +5 volts bias.

Three possible causes of the error current at high temperature are postulated:

1. ohmic leakage in the high temperature insulator
2. thermionic emission from hot cathode, giving apparent ion current increase
3. modification of the boundary layer profile toward higher n_e due to high wall temperature, i.e., temperature jump effect at the wall

We dispose of 3 immediately, since the error current is present with or without flow. (Temperature jump is discussed further in the final section.) Thermionic emission is not so easily discarded. Error current data of Figure 24 are plotted in Figure 25 to yield the effective work function. Assuming the current to be emission-limited (Ref. 15), (i.e., a high-vacuum diode),

$$ J = 60 \, T^2 \, e^{-\phi/kT} \tag{12} $$

whence

$$ \frac{d \ln J}{d(1/T)} = -\frac{\phi}{k} - 2T \tag{13} $$
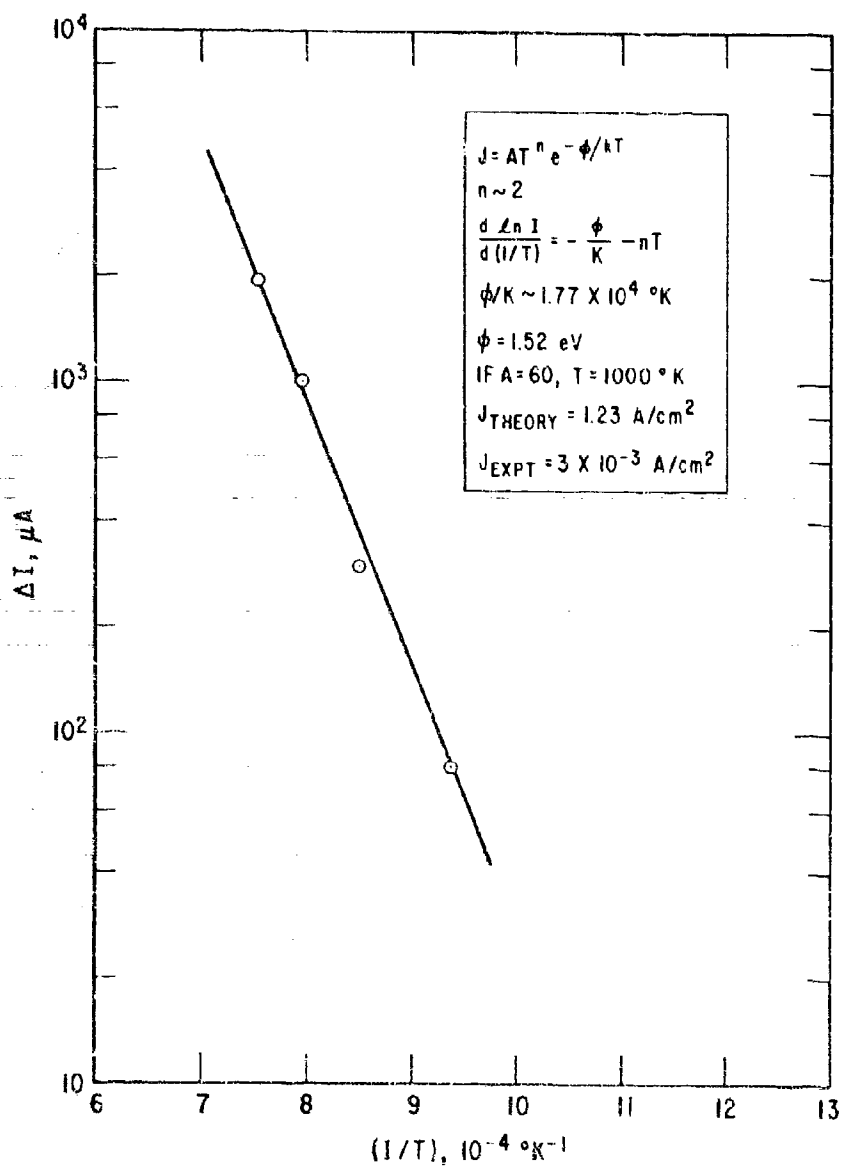
Figure 25. Determination of Effective Work Function
for Thermionic Emission as Possible Error
Current Source, Disc Probe

A value of $\phi = 1.52$ ev is obtained, an impossibly low work function. Even thoriated and oxide cathodes have work functions of 2 to 3 ev, and oxidized steels are expected to lie in the 3 to 4 ev range. However, this determination and the use of Eq. (12) are in question, since the actual current at several torr pressure will be diminished by space charge and mobility effects, but such modification can only result in requiring an even lower work function to explain the observed slope. If the error current is due to thermionic emission, then it will increase the apparent ion current; the conduction process must again be that of a mobility-limited diode between the two electrodes. In this case only the electron mobility is of concern. If we assume $K_e = 1000 \frac{cm}{sec} \frac{cm}{volt}$ at 1 atm, $V = 45$, $x = 1$ cm, and $p = 30$ torr, then (Ref. 15)

$$ J = \frac{9.95 \times 10^{-14} KV^2}{x^3} = 5 \times 10^{-6} \text{ amp/cm}^2 \qquad (14) $$

The actual leakage currents are of order 0.5 to 2×10^{-3} amp/cm^2 at a surface temperature of 1000°C. Hence, although the work function and predicted currents are both unreasonably small, we cannot entirely eliminate thermionic emission as a partial explanation of the probe error current. Chung's analysis is modified by emission in that the boundary condition $n_e = 0$ at the wall must be changed. However, unless the emission rate is so large that $n_{wall}/n_{peak} > 0.1$, no significant change in probe performance is predicted.[6]

Ohmic leakage through the insulator is the remaining, and most likely, possibility. If we consider the electrostatic analogy between capacitance and resistivity of two circular conductors in a semi-infinite medium (Ref. 26), then, for 0.4-in.-diam discs on 0.700-in. centers in a 0.1-in.-thick slab

---

[6]P. M. Chung, private communication.
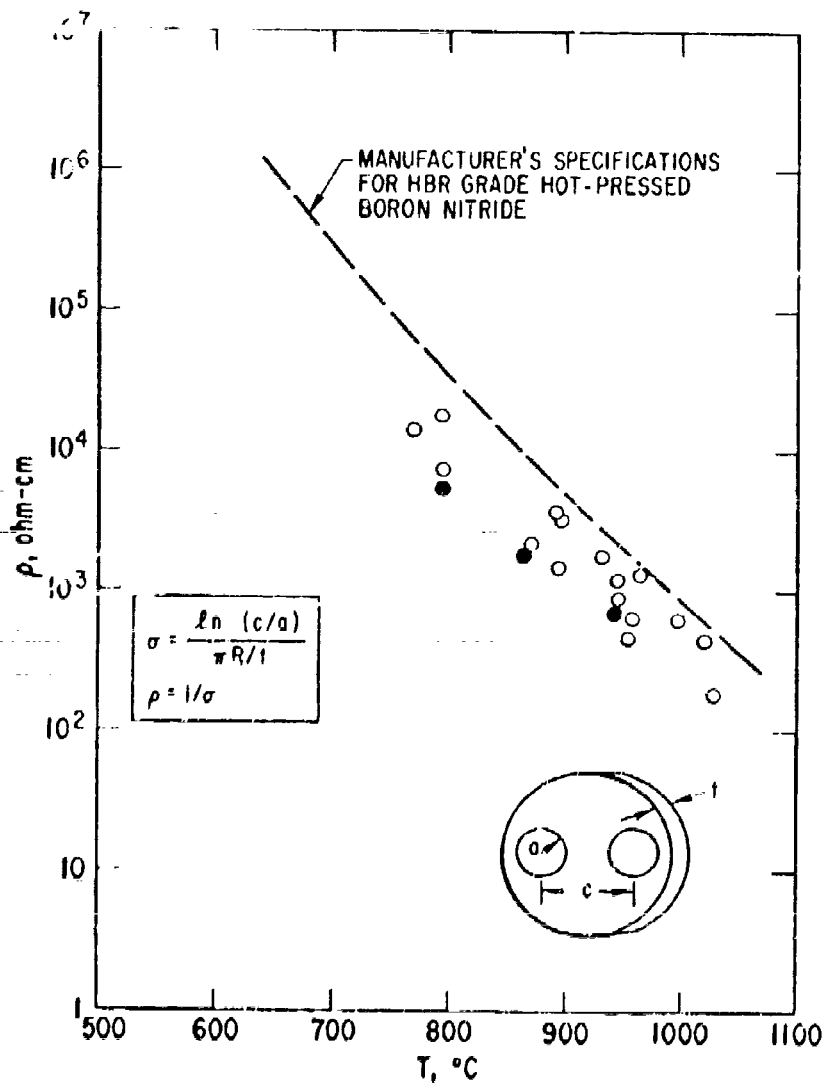
Figure 26. Effective Insulator Resistivity Derived
from Leakage Resistance vs Temperature,
Disc Probe

of boron nitride, we can evaluate the conductivity σ from (see Figure 26)

$$\sigma = \frac{\ell n \ (c/a)}{\pi R/t} \tag{15}$$

where $R = \Delta I/V_b$.

The resistivity $\rho = 1/\sigma$, derived from the experimental error currents and Eq. (15), is plotted in Figure 26 and compared with the manufacturer's specifications for HBR grade boron nitride. There seems little doubt that the leakage is almost entirely ohmic in origin. In order to check this hypothesis, we took further runs in which V_b was rapidly switched between 45 and 15 v as T increased. One would expect the error currents to bear the ratio 3:1 at a given $\sigma(T)$. The results, however, showed a ratio $\Delta I(45)/\Delta I(15)$ of about 1.5 at 800-900°C, rising to 2.0 at 1000-1100°C. Other effects may thus be contributing to the leakage current, but certainly, in an order of magnitude sense, the resistivity of the insulator limits probe operation to $T < 800°C$ for hot-pressed boron nitride. For the geometry chosen, with electrode dimensions and separation of the order of 1 cm, a resistivity of $\rho = 10^6$ ohm-cm seems the lower limit for error-free operation of the disc probe geometry. Recent data on pyrolytic boron nitride (PBN) in the direction parallel to the substrate shows resistivity about equal to that of beryllia. Then a PBN insulator at $n_{eo} > 10^{11}$ should be operable up to 1100°C without appreciable leakage.

One run was taken in which a BeO insulator was used. This BeO run is the last entry in Table 1 and is shown on Figure 23. It had 0.3 × 1-in. electrodes with the long dimension parallel to the flow and agreed perfectly with disc results below 600°C. Serious leakage current developed at 600°C and mechanical failure occurred at 1000°C, presumably due to thermal stresses. It is likely that the sample of BeO was not of optimum purity, since noticeable changes in color and grain structure were visible in the piece used. The poor thermal shock resistance and difficult machining qualities of BeO eliminate it from further consideration, since PBN is

electrically superior. In addition, the excellent match of PBN to the thermal, mechanical, and ablative properties of carbon phenolics makes it very attractive for composite high-temperature structures.

The effects of ablation contamination on probe performance were studied in two runs in which CP was permitted to ablate over a disc probe (Figure 15). The characteristics obtained duplicated those of the "clean" run of Figure 25, indicating that carbon phenolic pyrolysis and recession will not affect probes in flight. The CP sample shown in Figure 15 was thoroughly charred and showed a recession of 1/32 in. after the run up to 1000°C wall temperature.

IX.   PREDICTED FLIGHT PERFORMANCE

Complete performance curves for the flight performance of a flush probe will now be derived with the Chung and SRI models and the boundary layer structure of Figures 1-5. We assume a double probe biased at 45 v, with electrode dimensions 1×3 cm, separated by 1 cm, with long dimension parallel to the flow to minimize convection corrections. The insulator is PBN of 1 cm thickness. We assume that the insulator behaves like a semi-infinite solid and achieves a surface temperature given by the dotted curve on Figure 2, scaled down from CP by the ratio of $(\pi \kappa \rho \, \bar{C}_p)^{1/2}$. We consider two vehicles at 23 kft/sec, sharp 8-deg cones, one of Be and one of CP.

The boundary layer parameters are listed in Table 2. From these, using Eqs. (9) and (10), we calculated the Chung prediction of ion saturation current, which is shown in Tables 3 and 4. For Eq. (10), we note that $\rho_\delta / \rho_o \sim 5.8$ and $\mu_o / \mu_\delta \sim 3$, where $\mu_\delta = 3.6 \times 10^{-4}$ poise at 800°K, $u_\delta = 6.6 \times 10^5$ cm/sec, $x = 300$ cm, and $Sc_i = \ell = \eta_o = 1$. The parameter $\hat{A}$ is noted, and the theory may be considered valid only for $\hat{A} > 10^3$ [see Eq. (6)]. The results from Eqs. (9) and (10) differ by a factor 2, perhaps reflecting error in the assumptions used in deriving Eq. (10) from (9).

The SRI model results are also shown in Tables 3 and 4. We find the convection correction by assuming that the velocity and electron density profiles are given by

$$u = \frac{u_\infty}{2}\left[1 - \left(\frac{y_o - y}{y_o}\right)^2\right] \quad \begin{array}{l}\text{from peak } r_o \\ \text{to wall}\end{array}$$

$$n = n_s\left[1 - \left(\frac{d_s - y}{d_s}\right)^2\right] \quad \begin{array}{l}\text{from sheath} \\ \text{edge to wall}\end{array}$$

Table 2. Boundary Layer Parameters used for Flight
Performance Estimates[a]

h, kft	δ, cm	T_o, °K	p, torr	Δ, cm	ρ_o/ρ_{STP} $\times 10^{-3}$	ρ_δ/ρ_o	n_o Be cm^{-3}	n_o CP, cm^{-3}	y_o, cm
200	3.25	5000	3.1	0.16	0.35	6.25	10^5	2.8×10^7	0.4
175	2.1	4800	7.1	0.12	0.80	6.0	7×10^5	6×10^8	0.3
150	1.35	4680	15.5	0.085	1.6	5.85	2×10^7	2×10^{10}	0.275
125	0.8	4550	43.5	0.055	4.5	5.7	1.2×10^9	7×10^{11}	0.2
115	0.635	4450	68	0.045	7.9	5.55	7.5×10^9	3.5×10^{12}	0.175
100	0.4	4300	133	0.034	16	5.4	8×10^{10}	1×10^{13}	0.12

8 deg half-angle, sharp cone

$U = 21.8$ kft/sec

$T_w = 1000$°F

$T_\delta = 800$°K

$x = 300$ cm

$\mu_\delta = 3.6 \times 10^{-4}$ poise at 800°K

$\mu_o = 1.1 \times 10^{-3}$ poise at 4450°K

[a]Profiles from Figures 4 and 5, Ref. 4; peak electron density from Figure 1.

Table 3. Flight Performance of 1 × 3 cm Double Flush Probe on Carbon Phenolic Cone

h, kft	J/n_o Eq. (9), A-cm/e $\times 10^{-15}$	J/n_o Eq. (10), A-cm/e $\times 10^{-15}$	I Eq. (9), A	d_s, cm	n_s', cm^{-3}	v_s Eq. (4), cm/sec $\times 10^5$	J Eq. (1), A/cm^2	I_{conv}, Eq. (16), A	$I_{tot\ coll}$ Eq. (17), A	Â
200	7.05	10.1	8.4×10^{-7}	-	-	-	-	-	7.2×10^{-6}	1?
175	4.0	6.8	1.23×10^{-5}	0.32	6×10^{8}	1.67	3.2×10^{-6}	4.6×10^{-6}	1×10^{-4}	300
150	2.78	4.85	2.9×10^{-4}	0.09	1.7×10^{10}	1.67	1×10^{-4}	1.75×10^{-5}	-	3250
125	1.5	2.83	6×10^{-3}	0.024	3×10^{11}	1.31	1.57×10^{-3}	3.8×10^{-5}	-	-
115	1.03	2.15	2.2×10^{-2}	0.0095	2.35×10^{12}	1.05	9.4×10^{-3}	4×10^{-5}	-	-
100	0.665	1.51	4.5×10^{-2}	0.006	5×10^{12}	0.83	2.9×10^{-2}	-	-	-

Table 4. Flight Performance of 1 × 3 cm Double Flush Probe on Beryllium Cone

h, kft	J/n_0 Eq. (9), A-cm/e × 10^{-15}	I Eq. (9), A	Å	d_s, cm	n_s, cm^{-3}	v_s Eq. (4), cm/sec	J Eq. (1), A/cm^2	I_{conv}, Eq. (16), A	$I_{tot\,coll}$ Eq. (17), A
200	7.05	3×10^{-9}	-	-	-	-	-		2.6×10^{-8}
175	4.0	1.4×10^{-8}	-	-	-	-	-		1.16×10^{-7}
150	2.78	2.9×10^{-7}	4	0.8	-	-	-		2.1×10^{-6}
125	1.5	1.02×10^{-5}	120	0.15	$\sim 1 \times 10^9$	$\sim 1.7 \times 10^5$	5.8×10^{-6}	1.2×10^{-5}	7.6×10^{-5}
115	1.03	4.8×10^{-5}	400	0.065	$\sim 7.5 \times 10^9$	$\sim 1.5 \times 10^5$	4.3×10^{-5}	2.2×10^{-5}	3.8×10^{-4}
100	0.665	3.6×10^{-4}	2500	0.025	$\sim 8 \times 10^{10}$	$\sim 1.3 \times 10^5$	4.6×10^{-4}	1.3×10^{-5}	-

and that the convected electron current from wall to sheath edge is

$$I_{conv} = We \int_0^{d_s} nu\, dy = Wen_s \frac{u_\infty}{2} \left[\frac{5}{6} \frac{d_s}{y_o} - \frac{3}{10} \left(\frac{d_s}{y_o} \right)^2 \right] \qquad (16)$$

For cases where the sheath approaches the boundary layer thickness (given equivalently by $\hat{A} \sim 100$, $n_o \sim 10^9$, $d_s \sim y_o$), an approximate model of current collection is devised, assuming total collection of the convective flux over the probe. For the probe geometry assumed and $V_b = 45$, the mean local field is ~15 v/cm and fills the boundary layer to a distance W on either side of the ion collector. The ion drift velocity is given by

$$v_{drift} = KE \sim \frac{KV_b}{W} \sim 3 \times 10^5 \text{ cm/sec} \sim \frac{u_\infty}{2}$$

if DeBoer's value is used for K (Ref. 29). Diffusion velocity will be of order

$$v_{diff} \sim \frac{D}{n} \frac{dn}{dx} \sim \frac{D}{W}$$

where we assume the collector removes all ions over a dimension of order W. Then

$$\frac{v_{diff}}{v_{drift}} \sim \frac{D}{KV_b} \sim 0.02$$

(If we assume $D/K = kT/e$ and $T = 3500°K$, then $D/K \sim 0.3$, whence the result above.) Then, if the electrodes are at least twice as long as they are
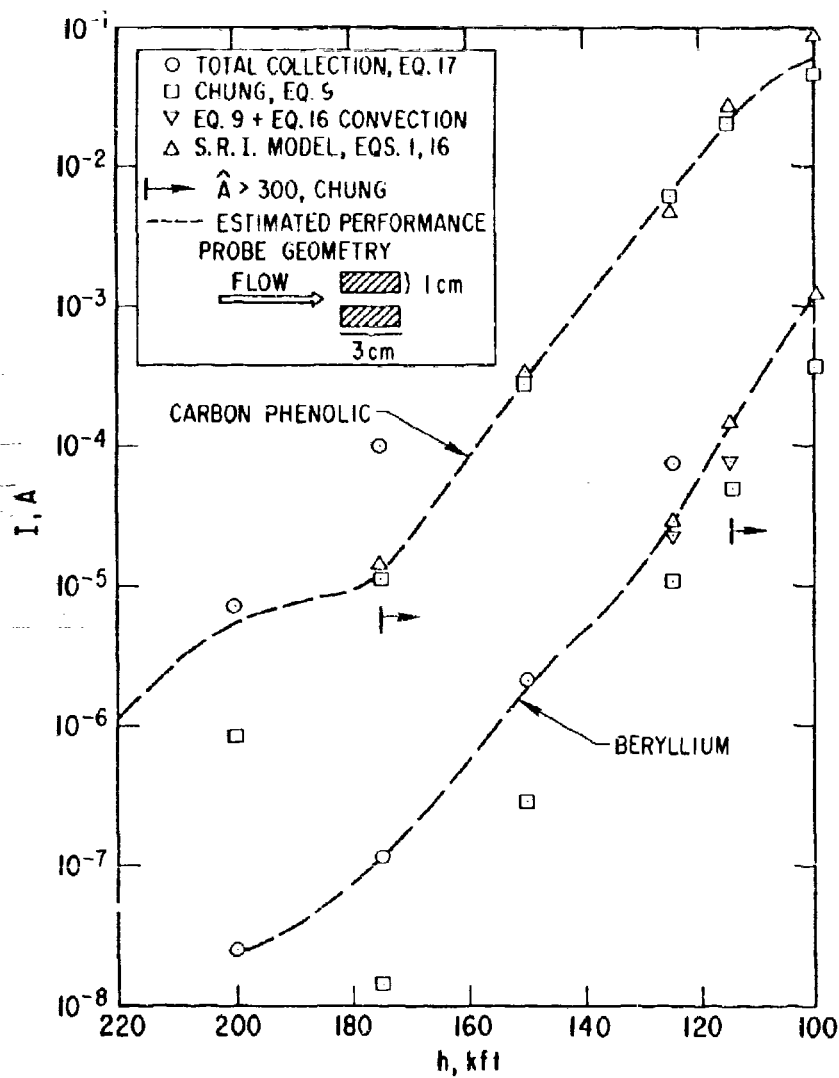
Figure 27. Flight Performance of 1 × 3 cm Double
Flush Probe on CP and Be Vehicles

wide, all ions in a width 3 W will be swept out, and no more will enter by diffusion. Then

$$I_{tot\ coll} = \frac{n_o}{2} \, 6 \, 3W \, \frac{u_\infty}{2} \, e \tag{17}$$

using average n_e and u over the boundary layer. This very crude estimate serves to extend the current collection prediction of Tables III and IV up to 200 kft, at least in an order-of-magnitude sense.

These calculations are summarized in Figure 27, where the Chung [Eq. (9)] and SRI results and the total collection results (assumed correct when $\hat{A} > 300$) are plotted vs altitude. Insulator leakage currents in PBN at presumed surface temperatures (Figure 2) are negligible compared to the ion currents. The expected overall flight performance is shown by the dotted lines. Chung's theory in the form of Eq. (9) is used, since it employs the boundary layer structure more directly. The almost exact agreement of the SRI and Chung models for CP cones is surprising but very encouraging, since they have been independently verified over the range of n_e expected in flight by Ref. 1 and this work, respectively. From 180 kft down to transition on blunt or "dirty" vehicles, we may thus expect to make good sense out of n_{eo} determinations from flight measurement of ion saturation current, using either theory. The convection corrections are negligible for the thin sheaths of contaminated CP vehicles. Clean air (Be heat shield) results are discouraging, however; only below 125 to 115 kft is either theory valid, and even then they disagree by a factor 2 or more. Since the SRI theory can explicitly handle a moderately thick sheath, it is presumed more correct than the Chung model for the beryllium vehicle case although both are on very shaky ground. Considerable hand-waving in the spirit of Eq. (17) seems the only data interpretation scheme currently available for clean air flights. Good laboratory simulation and calibration for $n_e < 10^{10}$ appear urgently required. The SRI shock tube results shown in Figure 19 do extend to 10^9,

but the empirical convection correction swamps the drift current at these levels, and an effective "total collection" model results.

Even with the apparently excellent prediction for success on CP veh' es, accuracy no better than a factor 2 should be expected. Possible systemat errors in the laboratory calibrations that have been done and, more important, the unknown factors that appear in the theory (such as Sc_i) do not permit any realistic confidence level closer than this.

The effects of temperature jump, where insulator and heat shield meet, have caused some concern in probe interpretation. If we consider that the diffusion of vorticity (i. e., boundary layer growth), heat, and molecular or ionic (ambipolar) species proceed at about the same rate when $Sc = Pr = Le = 1$, then the characteristic length for readjustment of the boundary layer profile or thickness to a temperature jump at x is itself x. Then, if we place the probe at position $x \gg \delta$ and limit its dimensions to a few B. L. thicknesses δ, any temperature jump should have no effect on the profiles in the vicinity of the probe. In an analytical study of the analogous problem of discontinuous surface catalycity in a reacting boundary layer, Chung[7] found that the boundary layer remains unaffected for many δ downstream of the surface discontinuity.

[7] P. M. Chung private communication.

X. CONCLUSIONS

Flush electrostatic probes with stainless steel electrodes in boron nitride insulators have been shown to operate successfully in a simulated high temperature reentry environment. For highly conducting boundary layers appropriate to Na-contaminated ablators or blunted vehicles, the theory of Chung (Ref. 2) has been found to correctly predict the electron density. The results are not sensitive to probe shape or orientation for the dimensions of order b employed and suggested for flight tests. Several important questions remain to be answered, particularly those involving uncertainty in Sc_i and the proper choice of theory and appropriate probe geometry for high altitude, low n_e situations, where the sheath and boundary layer are of comparable thickness. It is clear that the same probe geometry and the same theory cannot be used for both "dirty" and "clean" vehicles, since election densities and sheath thicknesses differ by 10^5 or so in the two cases. Some extension of the "total collection" scheme used by de Boer (Ref. 27), with very large electrodes to define the geometry clearly, offers promise. Further efforts are well worthwhile, since only the electrostatic probe, of the available techniques, has the sensitivity and dynamic range to cover the full range of electron densities of interest to the reentry physicist.

The present analysis has been limited to consideration of laminar boundary layers only. However, Chung (Ref. 2) indicates that his theory is applicable to the turbulent case if the appropriate fluid dynamic solution for the turbulent boundary layer is known, irrespective of the details of the chemical or electron density profiles. The major requirement is that the electron density be high enough to keep the sheath thinner than the fluid shear layer, which will usually be the case at the very high density, high surface temperature conditions obtaining below transition altitude. It is hoped that further laboratory tests in the turbulent regime can be carried out, as well as the urgently required calibration of probes for high altitude, clean air conditions where the current theories are inapplicable.

REFERENCES

1. H. R. Bredfeldt, W. E. Scharfman, H. Guthart, and T. Morita, Boundary Layer Ion Density Profiles as Measured by Electrostatic Probes, Technical Report 33, Stanford Research Institute, Menlo Park (February 1966); also AIAA J. 5, 91 (1967).

2. P. M. Chung and V. D. Blankenship, Electrostatic Probe for Electron Density Measurements on Reentry Vehicles, TR-669(S6240-10)-2, Aerospace Corp., San Bernardino (March 1966); also J. Spacecraft Rockets 3, 1715 (1966).

3. A. J. Pallone, J. A. Moore, and J. I. Erdos, "Nonequilibrium Nonsimilar Solutions of the Laminar Boundary Layer Equations," AIAA J. 2, 1706 (1964).

4. K. E. Starner and D. J. Spencer, An Arc Plasma Channel for Testing of Reentry Boundary Layer Instrumentation, TR-1001(2240-10)-5, Aerospace Corp., El Segundo (November 1966).

5. P. M. Chung, Weakly Ionized Nonequilibrium Viscous Shock Layer and Electrostatic Probe Characteristics, TDR-269(S4230-40)-1, Aerospace Corp., San Bernardino (July 1964).

6. K. E. Starner, Stagnation Point Langmuir Probe Measurements in a Supersonic Argon Plasma Flow, TDR-469(5240-10)-4, Aerospace Corp., El Segundo (February 1965); also AIAA J. 4, 1185 (1966).

7. R. G. Jahn, "Microwave Probing of Ionized Gas Flows," Phys. Fluids 5, 678 (1962).

8. S. W. Liu and K. E. Starner, Nonequilibrium Effects in Arc Jet Flow, TR-1001(2240-10)-2, Aerospace Corp., El Segundo (September 1966).

9. J. G. Logan and C. E. Treanor, Tables of Thermodynamic Properties of Air from 3000°K to 10,000°K at Intervals of 100°K, Report No. BE-1007-A-3, Cornell Aeronautical Lab., Inc., Buffalo (January 1957).

10. W. P. Thompson, M. Epstein, and C. J. Lenander, Microwave Breakdown of the Reentry Boundary Layer, TR-1001(2240-20)-11, Aerospace Corp., El Segundo (May 1967); also Proc. AMRAC, 23rd, University of Michigan (April 1967).

11. M. Katzin, A. D. Parsons, and D. L. Ringwalt, R-F Impedance Probe for Reentry Plasma Sheath Measurements, BSD-TDR-64-22, Electromagnetic Research Corp., College Park, Md. (December 1963).

12. A. E. Fuhs, O. L. Gibb, and W. R. Grabowsky, Use of R-F Bridge for Reentry Plasma Diagnostics, TR-669(6220-20)-4, Aerospace Corp., El Segundo (April 1966); also J. Spacecraft Rockets 4, 327 (1967).

13. F. F. Chen, "Electric Probes," in Plasma Diagnostic Techniques, ed. R. H. Huddlestone and S. L. Leonard, Academic Press, New York (1965), Chapter 4.

14. I. Langmuir and H. Mott-Smith, "Studies of Electric Discharges in Gases at Low Pressures," Gen. Elec. Rev. 27, 449 (1924).

15. J. D. Cobine, Gaseous Conductors, Dover Publications, New York (1958).

16. R. V. Churchill, Modern Operational Mathematics in Engineering, McGraw-Hill Book Co., Inc., New York (1944), p. 106 ff.

17. P. M. Chung, "Electrical Characteristics of Couette and Stagnation Boundary Layer Flows of Weakly Ionized Gases," Phys. Fluids 7, 110 (1964).

18. P. M. Chung, "Theory of Electrostatic Double Probe Comprised of Two Parallel Plates," AIAA J. 4, 442 (1966).

19. H. R. Bredfeldt, W. E. Scharfman, H. Guthart, and T. Morita, The Use of Ion Probes in Reentry Physics, Technical Report 26, Stanford Research Institute, Menlo Park (May 1965).

20. W. E. Scharfman, The Use of the Langmuir Probe to Determine Electron Densities Surrounding Reentry Vehicles, Final Report Contract NAS 1-2967, Stanford Research Institute, Menlo Park (January 1964).

21. S. C. Brown, Basic Data of Plasma Physics, M.I.T. Press, Cambridge (1959), p. 61.

22. P. M. Chung, Diagnostic Equations of Electrostatic Double Probes for Continuum Plasmas, TR-E5, Department of Energy Engineering, University of Illinois, Chicago Circle (December 1966).

23. R. Hoppman, <u>An Experimental Investigation of the Conduction of Electric Current between Cold Electrodes in Shock-ionized Air Plasmas</u>, TR AE 6605, Rensselaer Polytechnic Institute, Troy (July 1965).

24. A. Frohn and P. C. T. DeBoer, "Ion Density Profiles behind Shock Waves in Air," <u>AIAA J.</u> 5, 261 (1967).

25. C. W. Baulknight, "The Calculation of Transport Properties at Elevated Temperatures," <u>Transport Properties Gases, Proc. Gas Dyn. Symp., 2nd</u>, Evanston (1958).

26. G. P. Harnwell, <u>Principles of Electricity and Electromagnetism</u>, McGraw-Hll Book Co., Inc., New York (1949), p. 101, 42.

27. P. C. T. DeBoer, "Probe for Measuring Ion Density in a Slightly Ionized, High Speed Flow," <u>Rev. Sci. Inst.</u> 37, 775 (1966).

DOCUMENT CONTROL DATA - R&D

(Security classification of title, body of abstract and indexing annotation must be entered when the overall report is classified)

1. ORIGINATING ACTIVITY (Corporate author)	2a. REPORT SECURITY CLASSIFICATION
Aerospace Corporation El Segundo, California	Unclassified
	2b. GROUP

3. REPORT TITLE

EXPERIMENTAL EVALUATION OF FLUSH ELECTROSTATIC PROBES
FOR REENTRY MEASUREMENTS

4. DESCRIPTIVE NOTES (Type of report and inclusive dates)

5. AUTHOR(S) (Last name, first name, initial)

Thompson, W. Paul

6. REPORT DATE	7a. TOTAL NO. OF PAGES	7b. NO. OF REFS
July 1967	73	27

8a. CONTRACT OR GRANT NO. AF 04(695)-1001 b. PROJECT NO. F04695-67-C-0158 c. d.	9a. ORIGINATOR'S REPORT NUMBER(S) TR-0158(3240-20)-4 9b. OTHER REPORT NO(S) (Any other numbers that may be assigned this report) SAMSO-TR-67-14

10. AVAILABILITY/LIMITATION NOTICES

This document has been approved for public release and sale; its distribution
is unlimited.

11. SUPPLEMENTARY NOTES	12. SPONSORING MILITARY ACTIVITY Space and Missile Systems Organization Air Force Systems Command United States Air Force

13. ABSTRACT

The current collection characteristics of flush-mounted electrostatic probes
were determined in a simulated reentry boundary layer flow. The thermo-
chemistry and fluid dynamic profiles on sharp cones at 180 to 100 kft altitude
are simulated by a subsonic flow of arc-heated air in a $1/2 \times 2$ in. cooled
channel. The experimentally determined probe currents are correlated with
the known channel electron densities using two theoretical models developed
by Chung and Bredfeldt et al. It is found that for electron densities of order
$10^{10} - 10^{13}$ Chung's theory correlates the data well. High temperature mate-
rials were tested, and stainless steel electrodes in pyrolytic boron nitride
insulators are recommended for operation up to surface temperatures of 1400°
K. Comparison of the two theoretical models in predicting flight performance
shows them in excellent agreement for sodium-contaminated ablating cones
below 175 kft. For the low electron densities on sharp cones in clean air,
neither theory is valid above 115 kft altitude. Detailed graphs and tables of
flight environment, materials properties, and probe electrical characteristics
are presented.

14.

KEY WORDS

Boundary layer
Electrostatic probe
Ionization
Plasma diagnostics
Reentry

Abstract (Continued)

Best Available Copy